INL/EXT-18-52276
Revision 0

X-ray Diffraction (XRD) Characterization of U-10wt% Fuel Slugs from EBR-II Driver Fuel, FFTF Test Fuel, and AFC-4B and AFC-4D Testing in the Advanced Test Reactor

Kevin Tolman
Doug Porter

December 2018

The INL is a U.S. Department of Energy National Laboratory
operated by Battelle Energy Alliance

Idaho National Laboratory

INL/EXT-18-52276
Revision 0

X-ray Diffraction (XRD) Characterization of U-10wt% Fuel Slugs from EBR-II Driver Fuel, FFTF Test Fuel, And AFC-4B and AFC-4D Testing in the Advanced Test Reactor

Kevin Tolman
Doug Porter

December 2018

Idaho National Laboratory
Idaho Falls, Idaho 83415

http://www.inl.gov

Prepared for
TerraPower, LLC
Under CRADA 13-CR-13
And DOE Idaho Operations Office
Contract DE-AC07-05ID14517

X-ray Diffraction (XRD) Characterization of U-10wt% Fuel Slugs from EBR-II Driver Fuel, FFTF Test Fuel, And AFC-4B and AFC-4D Testing in the Advanced Test Reactor

INL/EXT-18-52276
Revision 0

December 2018

Approved by:

Kevin R. Tolman, Principle Investigator — 2/12/2019 — Date

Douglas L. Porter, 13CR13 INL Technical Lead — 2/12/2019 — Date

Gregory M. Core, 13CR13 Project Manager — 2/12/2019 — Date

CONTENTS

1. PURPOSE 1

2. BACKGROUND 1
2.1 Injection Casting Discussion and Previous XRD Results 2
2.1.1 Using Archive (Legacy) Samples as Standards 5
2.1.2 Current XRD Examination of Legacy U-Fs EBR-II Fuel 7
2.1.3 Final Testing of Legacy U-10wt%Zr EBR-II Fuel 9
2.1.4 Results 10

3. XRD Characterization of Fuel Used for AFC-4B and AFC-4D Testing in the Advanced Test Reactor 20
3.1 Introduction 20
3.2 History of XRD Measurements 20

Appendix A Extended Data for the Legacy EBR-II Fuel Slugs 23

Appendix B Extended Data for the AFC-4B and AFC-4D Fuel Characterization 31

Appendix C Setup and Analysis Parameters for XRD Characterization 33

FIGURES

Figure 1. Sketch of the injection casting process used to make EBR-II U-10Zr fuel. 3

Figure 2. SEM backscatter image of a cross section XRD sample, 1357 #8 of legacy EBR-II fuel. Note the "rind" at the surface, which appears in two grey shades—a silicide at the surface and a thicker carbide between the silicide and the fuel [1]. 4

Figure 3. UZr_2 concentration as a function of a diffracted x-ray intensity ratio, $I_{(110)}/I_{(021)}$. Note that lower ratios generally seem to be associated with rind and higher concentrations of UZr_2. 5

Figure 4. Unmounted legacy EBR-II U10Zr ID 1331, Sample 2, narrow beam (No.5). 6

Figure 5. XRD trace of U-5Fs sample showing six peaks. Left to right, the first small peak was unknown – fits UO2 (note overlay in [b]), the next three alpha U ([110], [021] and [002]), the next unknown – fits gamma U (note overlay in [a]) and last is (111) alpha – U peak [12]. 8

Figure 6. XRD legacy fuel data showing several peak height ratios, segregated by observation of rind or no rind, with background subtracted. The four different (geometry) slug types are also shown. 13

Figure 7. XRD peak height ratios for pairs of XRD scans on the same samples, six months apart. 14

Figure 8. XRD peak height ratios (PHR) for I(110)/I(021) with and without UZr_2 corrections. 16

Figure 9. Correction to I(110)/I(021) PHR as a function of uncorrected PHR. 17
Figure 10. XRD results for EBR-II legacy fuels comparing peak area ratio and peak height ration for the I(110)/I(021) ratios. 18
Figure 11. XRD results for EBR-II legacy fuels comparing peak area ratio and peak height ratio for the I(002)/I(021) ratios. 19

TABLES

Table 1. Analysis of ID 1331, Sample 2, unmounted and narrow beam (No.5). 6
Table 2. Peak height ratio I(110)/I(021) results using different background methods. All results are from use of the normal width x-ray beam. 7
Table 3. (From Table 2, reference [1]) Summary of results, using the sixth order Chebyshev polynomial background with FPF, for sample analysis. 10
Table 4. Typical data presentation for three XRD examinations. 12
Table 5. Comparision between XRD PHRs for standard transverse cross sections and orthogonally cut longitudinal cross sections 15
Table 6. Original AFC-4B characterization sample with XRD. 20
Table 7. AFC-4D initial/original XRD results. 21
Table 8. The I(110)/I(021) ratio comparing final sample polish techniques. 21

1. PURPOSE

Previous studies have shown that the irradiation growth behavior of uranium and uranium alloy fuels is dependent upon the presence, or lack thereof, of crystallographic orientation, otherwise known as the "texture," of the material. The purpose of this report is to document the x-ray diffraction (XRD) characterization of EBR-II and FFTF U-10wt%Zr driver fuel and the methods that have been developed to assess crystallographic texture of U-10wt%Zr. These legacy fuels were manufactured using an injection casting process and were demonstrated to have acceptable performance in EBR-II and FFTF. By characterizing the crystallographic properties of these fuels, a benchmark can be formed with which newly fabricated U10Zr fuels can be compared. For example, if new U10Zr fuels are made via alternate processing techniques, but are shown to have comparable crystallographic properties to the legacy fuels characterized herein, reasonable confidence can be gained that the new product will have acceptable in-reactor performance.

The secondary purpose of this study is to re-analyze characterization samples from ATR tests AFC-4B and AFC-4D. The samples were taken during fabrication of the experimental fuel pins. XRD examination of the fuel provided results difficult to explain. Now that the XRD methods have been revised, the further XRD exams can illustrate any differences with the original characterizations.

2. BACKGROUND

In an earlier report [1] it was explained that there was interest in a method to characterize U-10Zr fuel for potential crystallographic texture because uranium's historical characteristic of preferential thermal or irradiation growth is a given crystallographic direction [2,3,4]. If the material also has a preferential texture, then the growth in a given direction will manifest itself in a preferential direction defined by the fuel slug geometry and its texture. This could potentially lead to unexpected axial growth or shrinkage, or diametral growth, which could create stresses on the cladding holding in the fuel.

Such growth occurred in EBR-II fuel [5] in the U-5Fs composition where Fs is a mixture of noble metal fission products thought to be present after an early method of reprocessing. Five percent Fs consists of 2.4 wt% Mo, 1.9 wt% Ru, 0.3 wt% rhodium, 0.2 wt% Pd, 0.1 wt% Zr, and 0.01 wt% Nb. At some point in the fabrication history of U-5Fs fuel, a centrifuge was enlisted to help in the bonding process, where molten sodium is incorporated between the fuel and stainless steel cladding to make a good thermal bond. During irradiation, these fuel pins were found to grow axially in an unexpected fashion [4]. It was suspected that the stresses and heat treatment involved in the bonding process resulted in a textured fuel. An XRD exam was developed where the heights (intensities) of the XRD peaks at (110) and (021) were measured, and the I(110)/I(021) ratio was used to assess whether a [110], [001] texture was present.

In one of the reports written on this phenomenon [5], the authors mentioned why this ratio was chosen, specifically the reason for using the (021) peak in preference to the obvious (002) choice. They say, "The (002) is also distorted by contributions from the broad peak between 36.5° and 38.5°." This other peak is likely from a retained gamma phase, but they noted that it also could be from U_2Mo or U_2Ru. Regardless what causes it, it is not present in the U-10Zr spectra, so in the present case the (002) peak can be used.

After the problem caused by the centrifugal bonding, and after reverting back to the traditional sodium bonding technique, no other texture-related problems were observed or encountered for the EBR-II driver fuel, so eventually the XRD testing of production fuel was discontinued. The fabrication process became routine: injection casting, shearing to length, and sealing in stainless steel cladding with bonding sodium. The bonding process had reverted to the original light mechanical agitation. The mandatory XRD characterization for each batch of fuel was subsequently abandoned. Even as the driver fuel was

transitioned from U-5wt%Fs to U-10wt%Zr, there was no return to using XRD examination as part of fabrication control or as a required inspection.

However, recent thoughts to use alternate fabrication methods that impart crystallographic orientation have motivated research related to the XRD characterization as part of fabrication control. The injection-cast legacy U-10wt%Zr fuel had acceptable performance, and there is a great deal of test data available concerning its performance. Therefore, there was and is a need to have the material well characterized by XRD. Some of this has been done previously [1], but the present study characterizes a broader sample set of those legacy fuels, evaluates XRD in the orthogonal direction (relative to the fuel slug axis) in addition to the typical transverse direction, and utilizes updated and improved sample preparation and XRD data analysis techniques.

2.1 Injection Casting Discussion and Previous XRD Results

The legacy fuel was all injection cast. An earlier report [1] on these XRD studies explained the injection casting process but it is worth mentioning again, since it gives an indication as to why texture would not have been expected.

Figure 1 shows a sketch representing the various stages of the injection casting process. Simply, a bundle of quartz, closed-end, straw-like molds are positioned above the melt (a), a vacuum is applied and the molds are lowered into the melt (b), the furnace is re-pressurized with argon and the molds fill (c), and finally, the filled molds are lifted above the remaining melt (d).

Note that in the stage marked “c,” the molds had just been filled, and the lower end of the molds were still in contact with the melt. It is reasonable to expect that most of the fuel slugs had been cooled very quickly, all but the end where the melt was in contact before the mold pallet was lifted away from the melt (d). After the casting was completed, the molds were broken away, and the slugs were sheared to length, taking some of the quenched end furthest from the melt first and then cutting to length. In the process of the final cut, material from the unquenched/melt contact end was removed. It was this end that was suspected of having a “rind.” In many slugs it was possible that material that had been heated longer after casting was retained at that end of the processed fuel slug. That area may have developed a rind due prolonged contact with the quartz mold (causing zirconium silicide formation) and allowing carbon in the melt to react with zirconium and form carbides internally and in a surface layer. The surface reaction products are what make up the rind. A typical SEM backscatter micrograph of rind is shown in Figure 2.

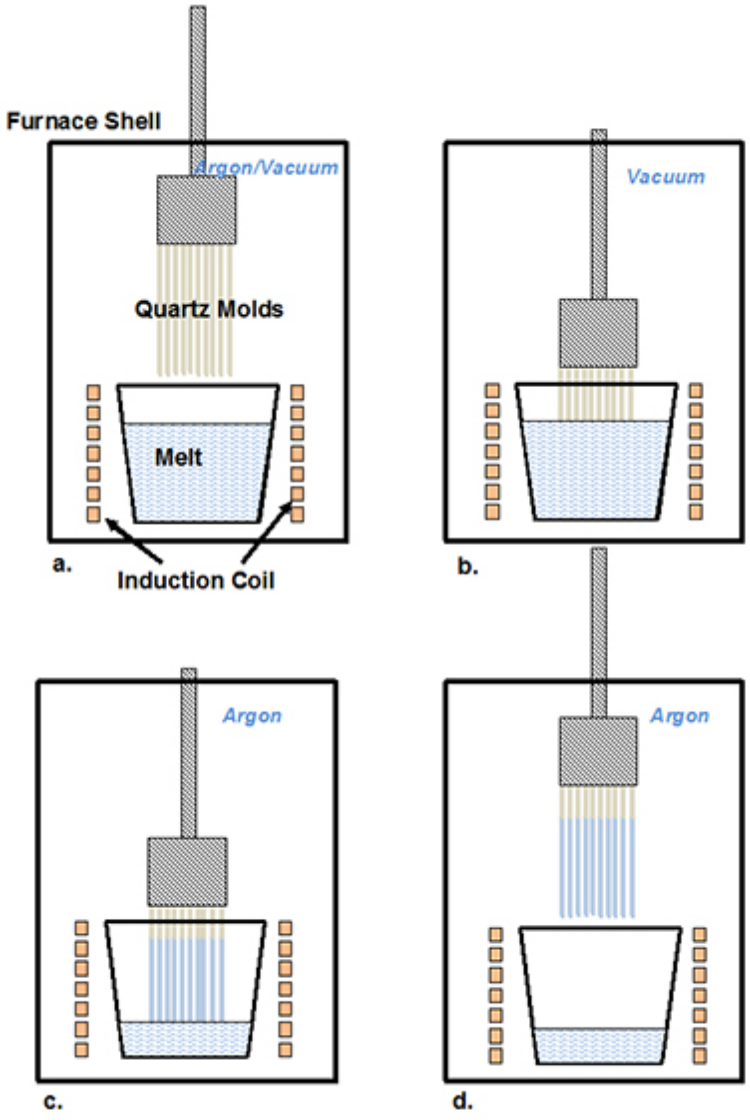

Figure 1. Sketch of the injection casting process used to make EBR-II U-10Zr fuel.

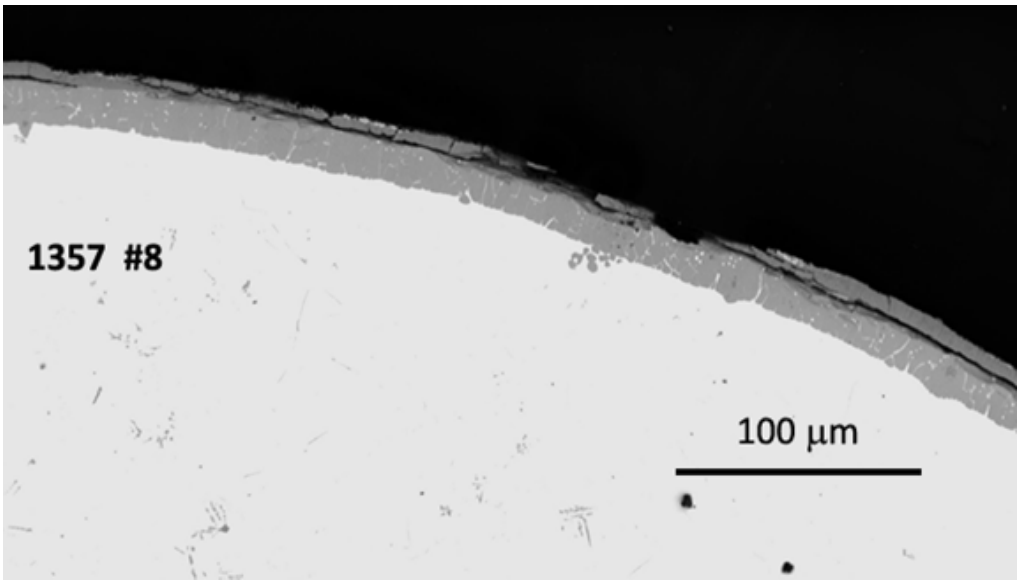

Figure 2. SEM backscatter image of a cross section XRD sample, 1357 #8 of legacy EBR-II fuel. Note the "rind" at the surface, which appears in two grey shades—a silicide at the surface and a thicker carbide between the silicide and the fuel [1].

Regardless of the source of the rind, one end of the fuel slug had this rind while the rest of the slug (>95% of the length) did not [7,8]. Since the XRD samples were taken from the two ends of the fuel slugs for the first sets of these archive samples, it was surmised that one end had been heated longer than the other and that perhaps that was the reason for observation of different XRD I(110)/I(021) ratios. Therefore, the surfaces of some of the samples from two of the batches were examined in the scanning electron microscope to reveal whether there was a correlation between the XRD information and the presence of the rind. Recall, however, that the XRD methods used today are different from the ones used for that report. Moreover, they set their peak height ratios using a cast rod of unalloyed uranium as the standard. There does appear to be a measured standard for uranium, even today.

In addition to the rind, it was suspected that the end nearest the melt in the crucible would also have a higher percentage of UZr_2, as the rest of the slug was cooled more rapidly and did not allow as much UZr_2 to form. Figure 3, taken from reference [1] shows that this theory may be true as rind and a higher UZr_2 content, with three exceptions, seem to be associated with a lower I(110)/I(021). The numbers may change somewhat today with the methods used to do the XRD examination. The new values will be shown subsequently in this report.

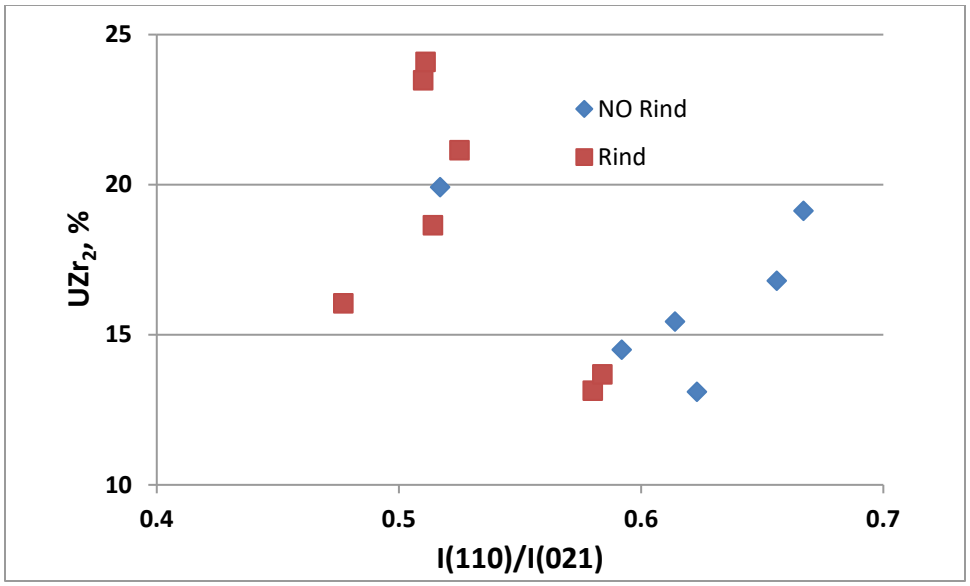

Figure 3. UZr_2 concentration as a function of a diffracted x-ray intensity ratio, $I_{(110)}/I_{(021)}$. Note that lower ratios generally seem to be associated with rind and higher concentrations of UZr_2.

In addition to testing samples without epoxy mounts, reference [6] also spent some time in examining the various calculation methods to look for texture, especially the Harris Method [9] and the March-Dollase Method [10].

2.1.1 Using Archive (Legacy) Samples as Standards

Details of the original attempts to ascribe texture, or the lack thereof, to U-10Zr are described in [1,6,13]. The pole figure method produced results that could not be interpreted because of the breadth of the diffracted intensity peaks. When peak height ratios were used, the $I_{(110)}/I_{(021)}$ ratios seemed low (0.5-0.65), as shown above. Perhaps the lower ratios were truly representative of non-textured U-10Zr. The lack of success in formulating a good figure of merit for a "texture/no texture" test prompted the suggested use of ratios obtained from legacy U-10Zr EBR-II driver fuel because thousands of U-10Zr pins were irradiated successfully in the 1980–1990s. It was believed, but not proven, based on the fabrication process used to make the fuel slugs, that they were non-textured or very minimally textured. At a minimum, their structure was adequate to provide acceptable and predictable performance in reactor.

The original studies of these materials [1], however, indicated that more refinements to the XRD techniques were necessary to produce consistent and trustworthy results. These were addressed in the next study [6], including mounting without epoxy, thus removing the background created by the epoxy mounts in which the samples were embedded. The background removal technique itself was also improved. In addition to testing samples without epoxy mounts, reference [6] also spent some time in examining the various calculation methods to identify texture, especially the Harris Method [9] and the March-Dollase Method [10]. When the improved method was finally chosen to run the XRD scan, a number of the legacy samples were examined using those methods. All XRD runs were done using a narrow and a "normal" beam for comparison, and the most important change was that they were all examined without an epoxy mount.

Figure 4 and Table 1 show a representative XRD characterization of one of the MK-IIC (#1331 samples) end pieces. Parameters used in this test during the last study of the legacy EBR-II fuel are essentially the same as those used in the current study.

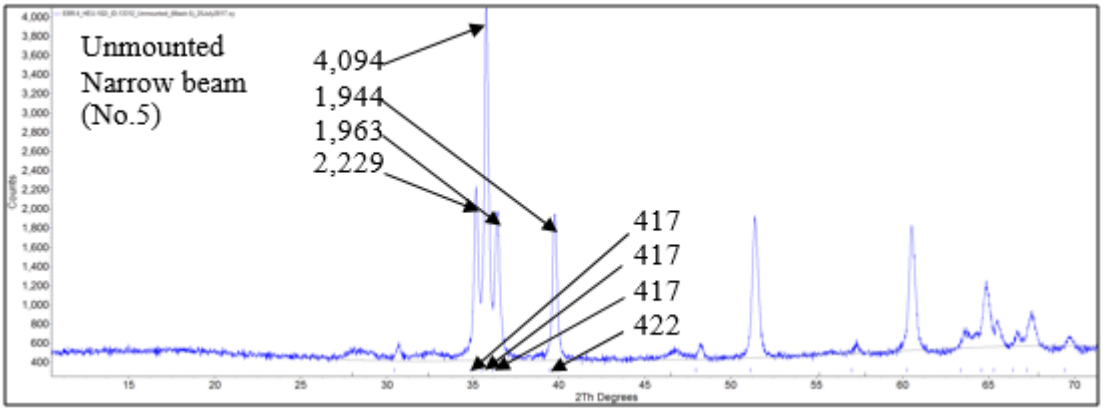

Figure 4. Unmounted legacy EBR-II U10Zr ID 1331, Sample 2, narrow beam (No.5).

Table 1. Analysis of ID 1331, Sample 2, unmounted and narrow beam (No.5).

Peak	(110)	(021)	(002)	(111)
Position (2θ)	35.19	35.78	36.41	39.75
α-U Intensity	2,229	4,094	1,963	1,944
Background at peak position	417	417	417	422
δ-UZr_2 Intensity	-	346	-	-
Net intensity	1,812	3,331	1,546	1522
Peak area	223.77	409.88	192.60	194.40
Peak intensity ratio I(110)/I(021)	0.544	-	-	-

The results for unmounted ID-1331, Sample 2, narrow beam showed a modified peak intensity ratio *I(110)/I(021)* of 0.544 (normal width beam ratio was 0.543) and a March-Dollase method *(110)/(021)* ratio of 0.801.

There were several of these unmounted samples that showed much lower $I_{(110)}/I_{(021)}$ ratios than the rest. While there was nothing specific that helped explain why, it was theorized that the sample preparation had allowed some of the deformed fuel alloy created by the shearing to remain in the near-surface region exposed to the XRD beam. Results like this served to somewhat confuse formation of conclusions regarding the study in [6].

A large number of samples were examined using various methods in [6]. One of the most impactful parts of the data analysis was background subtraction. Table 2, reproduced from [6], shows the change in the calculated I(110)/I(021) ratio. The first column shows results without background subtraction; the second using the background subtraction software in TOPAS (FP), which involved use of a sixth order Chebychev polynomial; and the third column shows results for which the separately measured backgrounds from the epoxy and the diffractometer were subtracted. The fourth column shows the ratio measured for an unmounted sample.

The last method was chosen. While there appear to be some merits in using the Harris March-Dollase Methods, this report will exclusively use peak height ratios or peak area ratios.

Table 2. Peak height ratio I(110)/I(021) results using different background methods. All results are from use of the normal width x-ray beam.

Background Method	No Background	FP-Background	Observed Background	Observed Background
Mount	Epoxy	Epoxy	Epoxy	Unmounted
ID13311	0.752	0.629	0.487	
ID13312	0.715	0.689	0.430	0.543
ID13313	0.724	0.660	0.350	
ID13314	0.777	0.673	0.438	
ID13315	0.734	0.568	0.391	0.530
ID13318	0.655	0.535	0.333	0.200
ID13319	0.718	0.607	0.388	
ID133110	0.745	0.631	0.455	
ID133111	0.708	0.519	0.325	

As a result of the previous work, the set parameters for running the XRD scans, as they are run now, and records collection for data and analysis are now contained in reference [11], the "Research and Development Test Control Plan (PLN-5527)" for these XRD analyses. Details of this and of the analytical methods used to analyze the XRD data are shown in Appendix C.

An original goal was to find a way to adapt the early U-5Fs XRD techniques and establish how the XRD results can be used for a specification to ensure lack of texture, namely I(110)/I(021) should be close to 0.75 or 0.78.

This may be a good place to reflect upon the use of the "traditional" peak height ratio I(110)/I(021) method as prescribed by Sturcken and others [3,5] in the 1960s. As previously mentioned in this report, it was interference between the retained gamma phase peak and the alpha (002) peak that required them to use the (110) peak instead. In addition, XRD methods in use in the 1960s were not nearly as sophisticated as they are today. We have shown how the choice of mounting material, or not mounting, has affected results. The computer-assisted methods of peak area generation, background subtraction, and others also modifies the results to some degree.

The standard uranium peak heights for the 1960s study was not a true standard, but another cast rod, using unalloyed uranium. In fact, the "card catalogue" standard values are calculated from what is known about the crystal structure. There are apparently few laboratory-generated standard patterns, and in one that was found [12], the measured PHR was 0.885, higher than the calculations. Of course, the limitations on methods and control of sample oxidation were higher in 1963.

One goal of this work was to perhaps generate that standard, using a hydride/dehydride produced powder specimen. The same XRD techniques used in this study would be applied to produce a non-textured standard of peak height ratios. However, this work was never completed.

2.1.2 Current XRD Examination of Legacy U-Fs EBR-II Fuel

A lot of effort went into trying to understand why the U-10Zr peak height ratios did not match the peak height ratios found in the 1960s studies. Plausible explanations included the presence of metastable phases and some differences in the structure of the alpha phase, as it contains a small amount of Zr. The

methods now versus then were also suspected. Recently, a manuscript was published showing an XRD scan of as-cast U-10Zr [15]. The work was done at a laboratory in India. The I(110)/I(021) looks to be ~0.45.

To test the theory that perhaps method changes may have resulted in the ratios being somewhat different, a piece of U-5Fs was found and examined [13]. The origin and history of the sample were unknown, but no other U-5Fs was available at that time to test. When the sample was first scanned, it appeared to be all retained gamma phase. It was heat treated as the U-Fs fuel pins had been to remove gamma phase (the sodium bonding treatment – ~1 hour at 500–550°C and slow cooled). The results are shown in Figure 5. Note that in Figure 5 (a) a peak has been added, representing a gamma-U peak that corresponds with one of the extra peaks. That peak interferes with the (002) alpha peak, making it not useful for testing for texture.

The conclusions, however, concerning the peak height ratios, were interesting in that the I(110/I(021) was 0.833, which fell just within the upper limit suggested for representing no growth impact from texture. The authors then said, "Note however that the ratios using the test methods/equipment here are in general slightly less than the methods used previously. A perfectly random texture was considered to be 0.79 but a ratio of 0.738(2) for relative intensities and a $I_{(110)}/I_{(021)}$ ratio of 0.702(1) for absolute peak intensities is considered random using this experimental set-up. The ratio measured here is slightly higher than would be considered perfectly random." So, their ratios were noted to be, in general, a little less than previously mentioned in the Sturcken literature.

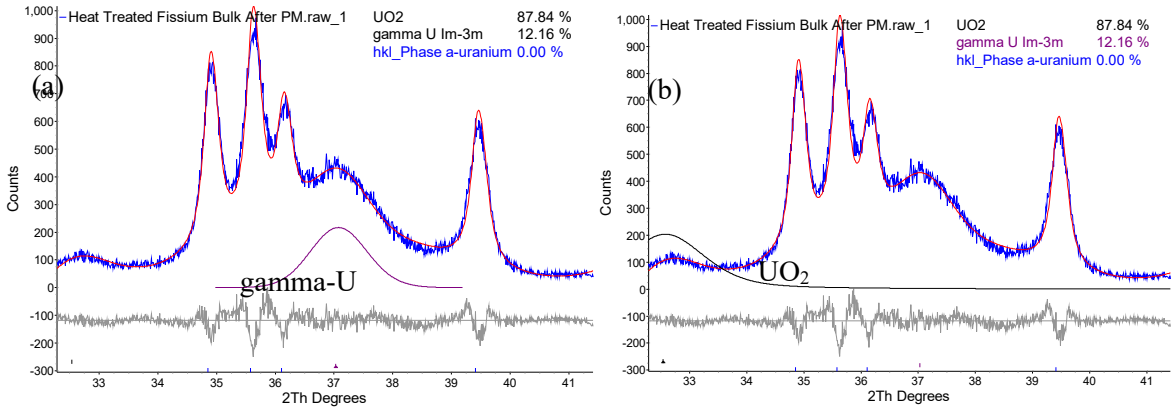

Figure 5. XRD trace of U-5Fs sample showing six peaks. Left to right, the first small peak was unknown – fits UO2 (note overlay in [b]), the next three alpha U ([110], [021] and [002]), the next unknown – fits gamma U (note overlay in [a]) and last is (111) alpha –U peak [12].

For the current study, an actual U-5Fs fuel pin (Mk-1A design) was de-clad using sodium evaporation. Two samples were taken for XRD analysis to see if the current XRD methods, when used on legacy U-5Fs slugs, could again produce the I(110)/I(021) peak height ratios, which would pass the old 0.74< I(110)/I(021) <0.84 specification [13].

The results of XRD characterization of two U-5Fs Mk-IA slug samples are shown in Appendix A. Transverse and longitudinal samples were studied. The I(110)/I(021) peak height ratios (PHR) for sample 1641T and 1642T were 0.656 and 0.564, respectively. For the longitudinal samples 1641L and 1642L, the ratios were 0.583 and 0.593. These values are less than theoretical, but orthogonally cut samples show no sign of texture. In addition, they would NOT have passed the original specification.

Using peak area ratios, the values for PAR (110)/(021) were 0.725 and 0.657 for 1641T and 1642T, and 0.0.665 and 0.688 for 1642L and 1642L. The values are larger, but still somewhat less than theoretical and, again, showed no sign of texture.

2.1.3 Final Testing of Legacy U-10wt%Zr EBR-II Fuel

The first three sets of samples (EBR-II driver fuel types MK-III, MK-IIC, and MK-IV) were obtained from the same samples cut from the slugs in the previous work [1,6]. The sheared ends had been split in half by sawing to expose surfaces that had not been deformed by the shear. As such, two samples of each sheared piece existed: one used in the original studies and one used for this work. In addition fresh samples were taken from slugs reclaimed from pins produced for a Fast Flux Test Facility (FFTF) experiment, MFF-8A. Each of the four fuel pin designs used were of different fuel slug diameter with MK-IIC, 3.30 mm; MK-IV, 4.27 mm; MK-III, 4.39 mm, and MFF-8A, 4.98 mm.

Five fuel slugs had been selected from each of the four designs and samples had been taken from each end of each fuel slug, so the process began with ten samples of each type. MFF-8A FFTF fuel samples were added (10 samples) to the re-purposed samples from the Mk-III, Mk-IV, and Mk-IIC batches. Each of these had nine samples in their respective batches. As such, the current study represents 37 samples from 20 fuel slugs recovered from fabricated fuel pins. Note that the orientation of the fuel slug was not maintained here, nor was it when the pins were fabricated. In other words, there is no way of knowing which end of the casting was represented by these two samples from each slug.

The XRD results presented here are not repeated from previous studies, but there are several campaigns of XRD characterizations reflected here, utilizing some of the same samples and, ostensibly, the same experimental techniques. One campaign was in 2017 while the XRD apparatus was stationed in INL's Analytical Laboratory. Another was completed in 2018 when the XRD equipment was located in the Irradiated Materials Characterization Laboratory, after the XRD test plan had been produced. The results are marked with the month and year that they were performed. Note also that the Mk-III samples all have a "1357" in the sample number; likewise Mk-IV have "1347," Mk-IIC have "1331," and MFF-8A have "1603." Please note that the data collected in 2018 were done to a Test Plan, "X-Ray Diffraction Texture Analysis of Uranium Alloy Fuel," PLN-5527, Rev. 0 (1/15/2018) written in compliance with PDD-13000, "INL Quality Assurance Program," and PLN-4553, "Quality Assurance Program Plan for TerraPower, Metallic Fuel, and Materials and Development."

The data will be shown comparing I(110)/I(021) or I(002)/I(021), comparing the ratio formerly chosen to study U-5Fs with one that may be more representative of the texture components. The texture described fits that for the mechanical deformation induced texture in BCC metals (the crystal structure for γ-uranium). It is expected, and observed, that such deformation creates a preferred alignment of the (002) planes. When the fuel sample is aligned so that the XRD examines the face of a sample cross-cut perpendicular to the direction of deformation, the (002) is exceptionally prevalent (reflecting a high intensity). So, in this case (U-10Zr), because there is no major second phase interference at the (002) positon, and especially in regards to elimination of the texture created by high-T deformation, it is recommended that the (002) be used to assess the anisotropy of the U-10Zr samples. This report contains a comparison of this method with the $I_{(110)}/I_{(021)}$ used previously.

2.1.3.1 Sample Retrieval Effects on "Legacy" Status

These 37 samples were supposed to represent the same fuel that had been used and studied during the operational days of the EBR-II and FFTF reactors. Indeed, the samples were taken from fuel that had been fabricated for such use, to specifications written for those fuel types. However, the fuel slugs were

subjected to a process that other production fuel had not been subjected to. The fuel had been removed from the stainless steel cladding by opening an end and evaporating the sodium bond within.

The process to remove the sodium was to open the ends of a group of pins, load them into a sealable pipe in the center of a chamber containing heating elements, start to obtain a vacuum in the pipe, and then provide power to the heating elements near the pipe. The thermocouple (TC) used to measure the operation temperature was attached to the outside of the pipe. A 650°C temperature was achieved, and the sodium was evaporated. The temperature was maintained for more than 3 hours.

The TC attached to the pipe provided a conservatively high measure of the fuel pin temperatures, but there was no internal TC to measure how conservative it was. The conservatism comes from not knowing the heat balance as the sodium is being evaporated.

If the temperature were 650°C, then this should be in the $\alpha+\gamma_2$ regime instead of the cooler $\alpha+\delta$ regime. Depending on the phase diagram, the transition between these occurs at just over 600°C. Transforming the delta to gamma phase seems it may create a microstructure that may be less restrictive to things such as grain growth.

The bonding temperature specified for EBR-II fuels was "not to exceed 540°C." It is not clear why this temperature was set. The most recent bonding treatment was at 600°C.

One small piece of information that may help to identify possible alterations caused by this is the previous examination of three fuel slugs [7, 8]. These fuel slugs were reclaimed from unused fuel pins without the use of heat; the sodium was washed away with alcohol. The XRD results, although not done using exactly the same methods as used currently, were similar between these samples and the legacy samples tested using the older methods. The table reproduced below from reference [1] are the XRD results from characterizing those samples; the values are the I(110)/I(021) peak height ratios for transverse and longitudinal versions of two samples. These are not unusual values compared to those being obtained during that period using the methods used at that time. For instance, the set of thirty-one legacy samples showed I(110)/I(021) PHR values of 0.477 to 0.667, with an average of 0.565, lower than those below. However, the results showed a bimodal distribution among those with the higher ratio similar to these two/four samples.

Table 3. (From Table 2, reference [1]) Summary of results, using the sixth order Chebyshev polynomial background with FPF, for sample analysis.

Sample Origin	Composition	% Reduction from Rolling	CS	T	L
R1A2 R1A5A	U10Zr	0	NA	0.625 ± 0.015	0.602 ± 0.016
RA2 RA5A	U10Zr	0	NA	0.627 ± 0.027	0.553 ± 0.013
R1C2 R1C5A	U10Zr	0	NA	0.621 ± 0.027	0.615 ± 0.014
R2C2 R2C5A	U10Zr	0	NA	0.622 ± 0.023	0.636 ± 0.013
R2A2 R2A5A	U10Zr	0	NA	0.639 ± 0.024	0.620 ± 0.014

2.1.4 Results

Table 4 shows an example of the results presented for three XRD examinations of legacy samples. They all represent the technique developed in [6].

There are only three shown here, but all are given in Appendix A. Note that the three represent MK-III fuel samples, two of them 1357A and 1357B. 1357B is shown twice, as the sample was examined twice. It was examined once before the test plan [11] was written and once after, when it was thought all

should be re-run. The data were kept, as they help to present as sense of repeatability. Note that the surfaces were re-ground and polished between examinations.

Table 4. Typical data presentation for three XRD examinations.

ID	Date	Goniometer Radius [mm]	Generator [kV]	Generator [mA]	Temp. [˚C]	2θ [20˚ - 90˚]	Step Size	Step Time [sec]	Solar [rad]	Mask	Slit Size [mm]	Cu Kα1 [Å]	Spinning	α-U %	UO2 %	d-UZr2 %
1357A	Aug'18	240	45	40	25	Y	0.013	198.645	0.4	10	0.1	1.5406	Y	87.44	3.51	9.05
1357B	Apr'18	240	45	40	25	Y	0.013	198.645	0.4	10	0.1	1.5406	Y	81.29	6.4	12.32
1357B	Nov'17	240	45	40	25	Y	0.013	198.645	0.4	10	0.1	1.5406	Y	82.79	7.07	10.15

		Calculated patterns w/o Texture																		
		Random Simulated NORM	(110)	Random Simulated NORM	(021)	Random Simulated NORM	(002)	Random Simulated NORM	(111)	Random Simulated NORM	(112)	Random Simulated NORM	(131)	Height	Height	Height	Height	Height	Height	Height
ID	Date	Calc.(110)	Obs. Bkgnd	Calc.(021)	Obs. Bkgnd	Calc.(002)	Obs. Bkgnd	Calc.(111)	Obs. Bkgnd	Calc.(112)	Obs. Bkgnd	Calc. (131)	Obs. Bkgnd	Obs.(110)	Obs.(021)	Obs.(002)	Obs.(111)	Obs.(112)	Obs.(131)	Sigma +/-
1357A	Aug'18	11147.24	2064.127	16669.36	2064.13	8773.244	2089.93	8747.44	2167.345	7847.903	2593.218	6679.692	3011.723	6708.9	14837.25	9805.416	7818.485	7847.903	7583.769	
1357B	Apr'18	12255.89	869.5482	17650.96	868.412	9877.388	867.611	8827.409	864.1865	7032.066	863.5921	5310.644	870.0039	7583.741	16207.82	10637.35	7411.725	7542.56	5789.536	76.000
1357B	Nov'17	13734.18	869.1419	19617.37	869.142	10686.27	869.142	9989.733	858.5302	7868.195	852.5623	5942.031	850.9452	8063.642	18589.58	14974.61	8418.959	9081.542	5893.172	95.333

		Card(110)		Card(021)		Card(002)		Card(111)		Card(112)										
		Catalog#	73	Catalog#	100	Catalog#	51	Catalog#	54	Catalog#	41									

								Peak Area Ratios (PAR)			Peak Height Ratios (PHR)			PHR w/o delta phase correction	PHR w delta phase correction
ID	Date	Area Int.(110)	Area Int.(021)	Area Int.(002)	Area Int.(111)	Area Int.(112)	Area Int.(131)	Area Ratio I(002)A/I(110)A	Area Ratio I(110)A/I(021)A	Peak-Height (110)_(021)	Peak-Height I(110)/I(021)	PHR I(110)/I(021)	PHR I(002)/I(021)	I(110)/I(021)	I(110)/I(021)
1357A	Aug'18	176.262	449.931	264.633	266.057	452.993	623.518	1.501	0.392	0.3636	0.3636	0.364	0.604	0.3636	0.3636
1357B	Apr'18	117.549	321.105	190.003	171.111	380.227	517.202	1.616	0.366	0.4377	0.4377	0.438	0.637	0.4377	0.5050
1357B	Nov'17	121.546	334.465	252.674	183.095	438.180	500.944	2.079	0.363	0.4060	0.4060	0.406	0.796	0.4060	0.4553

All of the legacy data gathered are shown in Figure 6. The added feature is whether the rind was observed on the sample's surface using optical metallography of a transverse cross section. Unlike the original study of legacy slugs [6], there doesn't appear to be correlation of low I(110)/I(021) ratio with the observation of the rind.

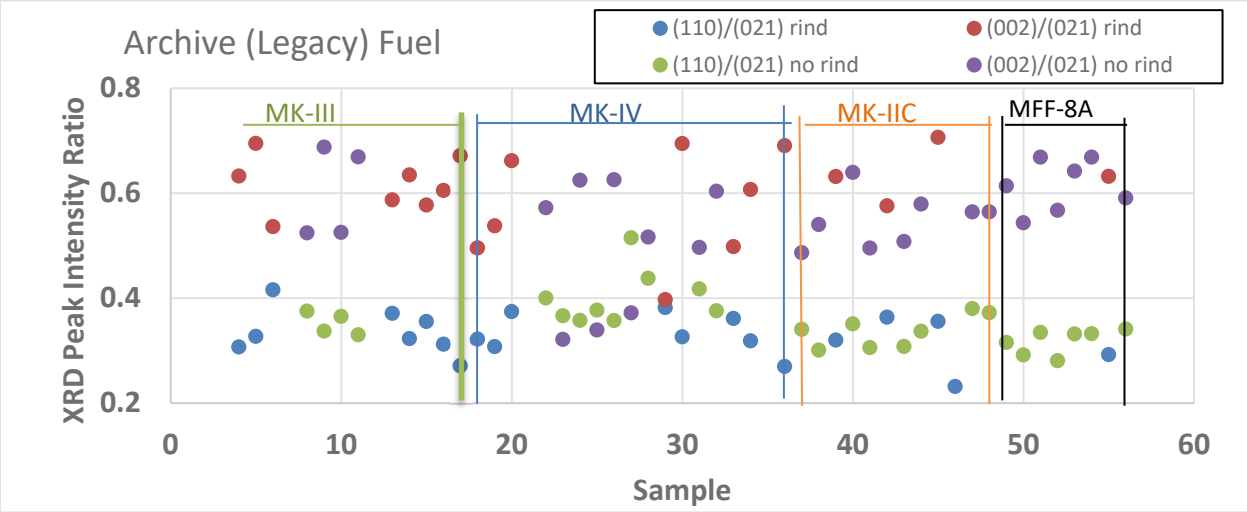

AVG	0.329	0.631	0.355	0.554
	110/021 R	002/021 R	110/021 NR	002/021 NR

Figure 6. XRD legacy fuel data showing several peak height ratios, segregated by observation of rind or no rind, with background subtracted. The four different (geometry) slug types are also shown.

There were multiple runs for most of the samples. The original scans were done in October–November of 2017, before the XRD test plan had been written. It was then decided to run them again after the test plan was written for quality purposes; this was completed in March–April of 2018. A benefit of this was seeing how the same sample, re-polished and re-examined by XRD, using the same equipment and operating parameters, repeated. These exams were done about six months apart.

Figure 7 shows the data pairs, where each pair represents the same XRD sample in both 2017 and 2018, re-polished and re-scanned in the second set of tests (2018). Two different peak height ratios, I(110)/I(021) and I(002)/I(021), were examined in each test. Looking more closely at the pairs of data, the first question to answer is whether this variation in results arises from an inherent scatter in the data or whether something changed in the samples or in the analysis of them.

The data do seem to partition into the 2017 data and the 2018 data, with the I(110)/I(021) ratio being higher in 2018 than it was 2017 and the I(002)/I(021) being higher in 2017 than it was in 2018. A trend like this indicates that something was done differently in 2017 than in 2018, perhaps sample preparation. General scatter in the data does not explain this.

The point is that there seems to be something less controlled than desired, despite the control provided by the XRD test plan. One way to avoid this problem is to prepare a control with each set of samples run, a sample that has been examined a number of times. Small variation in something like sample preparation would then reset goal ratios for that set of fabricated materials. Of course, alternatively, further study may uncover the cause of the difference in the results when the sample sets are re-scanned. Discovery of the cause may direct the way to remove it as a variable.

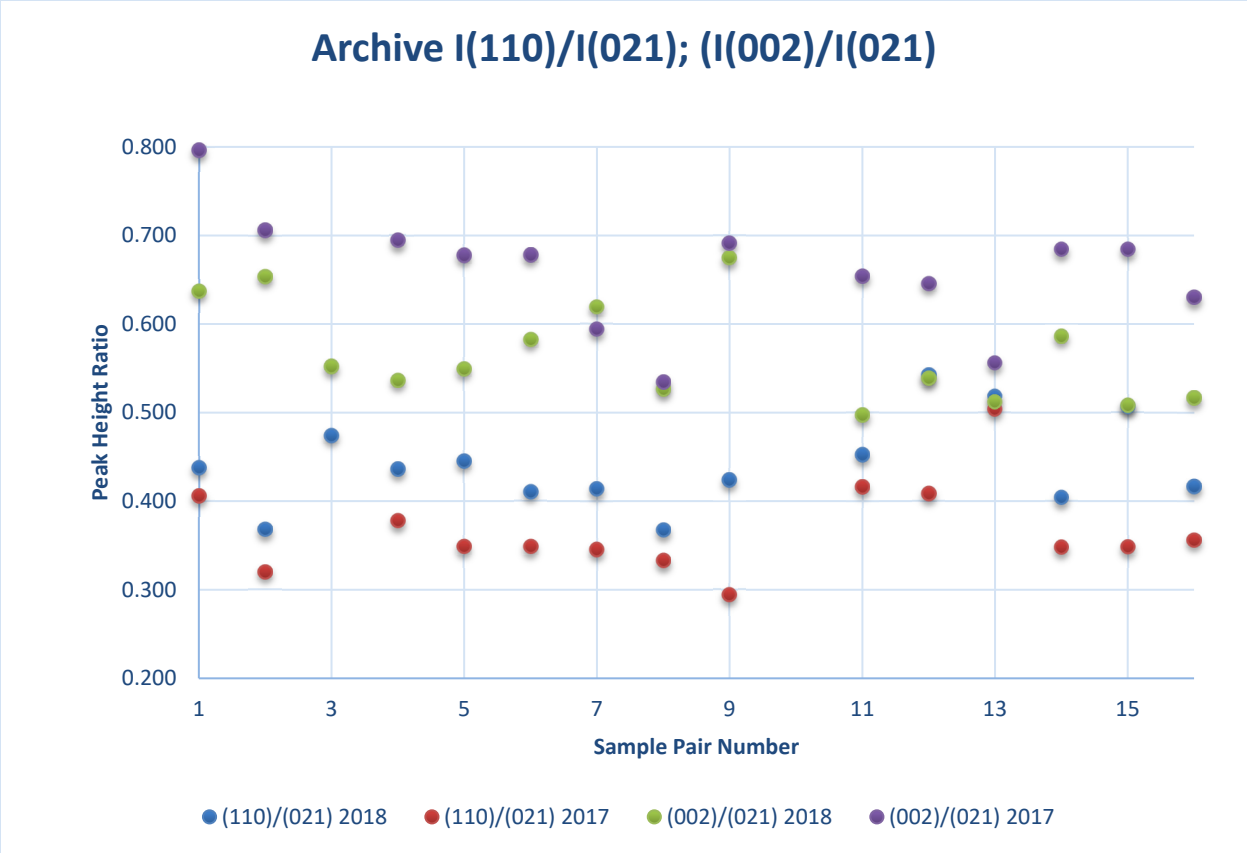

	I(110)/I(021)		I(002)/I(021)	
AVG	0.441	0.368	0.566	0.659
Sample Set	2018	2017	2018	2017
STD	0.051	0.052	0.057	0.066

Figure 7. XRD peak height ratios for pairs of XRD scans on the same samples, six months apart.

Interestingly, the observation of rind or no-rind was consistent for all pairs of exams. Again, however, there seemed to be no correlation between the existence of the rind and the peak height ratios as had been noticed in reference [1].

Note that the average and standard deviation for the I(110)/I(021) ratio and for all samples was 0.400 and 0.064 respectively. For I(002)/I(021), the average and standard deviation was 0.617 and 0.076.

2.1.4.1 Orthogonal/Longitudinal Cross Section Samples

In order to fully describe the potential crystallographic texture, or lack there of, of the legacy U-10Zr cast materials, there were some XRD samples cut as longitudal cross sections of the portion of the fuel slug. If they have the same PHRs, then there is go reason to believe that the slug is not textured.

Table 5 shows the rests of testing those samples compared to the transverse samples already mentioned. Note that the 1347 samples (Mk-IV) all show very little difference between the orthogaonally cut samples. Perhaps the I(002)/I(021) ratio is the least best fit of the three ratios shown.The XRD results for the one 1331 (Mk-IIC) sample, 1331-F, show more variation between the two orthogonally cut samples.

Table 5. Comparision between XRD PHRs for standard transverse cross sections and orthogonally cut longitudinal cross sections

LEGACY			
	PHR	PHR	PHR
Longitudinal Comp for Legacy	I(002)/I(110)	I(110)/I(021)	I(002)/I(021)
ID-1331-F-XRD-L	2.128	0.470	0.617
HEU-10Zr Pin 1347-2-1-XRD-L	2.776	0.360	0.417
HEU-10Zr Pin 1347-2-2-XRD-L	2.675	0.373	0.452
HEU-10Zr Pin 1347-2-9-XRD-L	2.511	0.398	0.460
Average	2.444	0.414	0.513
	PHR	PHR	PHR
Transverse	I(002)/I(110)	I(110)/I(021)	I(002)/I(021)
HEU-10Zr Pin 1347-2-1	2.724	0.367	0.526
HEU-10Zr Pin 1347-2-2	2.359	0.424	0.674
HEU-10Zr Pin 1347-2-9	2.399	0.416	0.516
1331-F	3.615	0.277	0.521
Average	2.774	0.371	0.559

2.1.4.2 Analyses to Identify Methodlogy to Assess Lack of Texture

Now that the data have been shown quickly, there are choices to be made to pick a simple method for using the data to assess lack of texture, which is the reason all of this was done in the first place.

2.1.4.3 Corrections for the Presence of UZr_2

The steady-state phase constituents in U-10wt%Zr at room temperature include alpha uranium (α) and UZr_2or delta (δ) phase. While there are many others phases that may participate in a metastable state, and these can very much contribute to misunderstanding the overall XRD description of the material, the two phases that would be expected if the materials were properly heat treated to remove the metastable phases are just the α, its variants, and the δ phases. The δ phase usually appears in a lath structure with the majority α phase. As such, whether forming after texturing or before, it is reasonable to assume the δ is textured if the uranium is textured.

This latter aspect could make the correction of the XRD peaks more difficult as the texture in the δ also needs to be characterized. This study does not take that nuance into account. For this study, the analysis involves finding a peak associated with the δ phase, and then the program uses card catalogue peak height ratios to estimate the peak height of a peak which interferes with one of the uranium peaks. It then subtracts that amount from the measured peak.

Figure 8 shows the I(110)/I(021) ratio with and without the corrections for existence of the δ phase. The corrections seem to be fairly consistent from sample to sample, increasing the I(110)/I(021) with the correction being done. The interference between the δ phase and alpha uranium is δ – (110), (101) at 35.7°2θ and α – (021) at 35.6-35.7°2θ. For the legacy fuel data, the increases are fairly consistent, likely due to the consistency in the fabrication method.

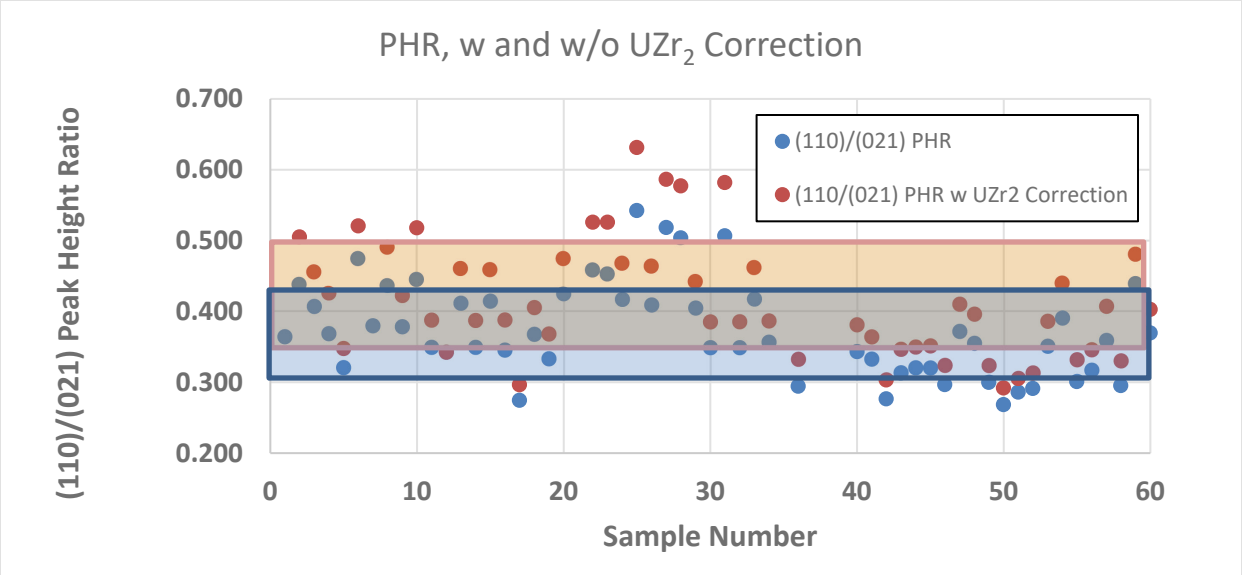

Average	0.372	0.415
STDEV.S	0.066	0.083
	No correction	w UZr_2 correction

Figure 8. XRD peak height ratios (PHR) for I(110)/I(021) with and without UZr_2 corrections.

Observations of this data perhaps indicate that the correction is fairly regular, with the corrected values being higher. The amount of correction seems to be greater when the uncorrected ratio is larger. There is likely a reason for this as the MK-IVs, Samples 18–36, were the last slugs made in this series, so there may have been a slight change in, for example, casting procedure. The bonding step or the de-cladding step may have been slightly different, but regardless, the amount of correction seems to be consistent with the original ratio value. Figure 9 shows the consistent increase in the UZr_2 correction to the I(110)/I(021) PHR as the uncorrected ratio increases. The steadily increasing correction seems to indicate, if caused by a fabrication variation, that there was a continuous change in the variable that instigated the change in ratio.

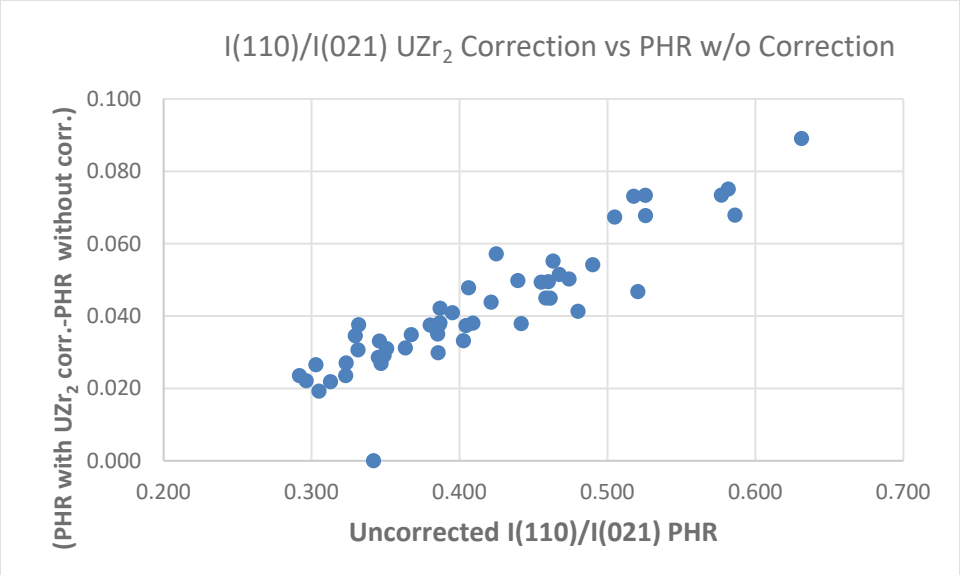

Figure 9. Correction to I(110)/I(021) PHR as a function of uncorrected PHR.

2.1.4.4 Peak Area Ratio (PAR) vs. Peak Height Ratio (PHR)

The effect of calculating areas under the peaks (perhaps necessary when there are a variety of fabrication variables) on variations in physical characteristics such as grain size, can be analyzed by looking at the peak area ratios (PAR) versus the peak height ratios (PHR). As with corrections for UZr_2 the effects may be the same for all samples with the same fabrication history.

Figures 10 and 11 show the comparison of PHR a versus PAR for the I(110)/I(021) ratio and I(002)/I(021) ratios, respectively. While there are some changes in the I(110)/I(021) and I(002)/I(021) values dependent upon whether the peak height ratio or the peak area are used, the standard deviations do not seem to be reduced by using the PAR instead of the PHR. The standard deviation for the PAR for the I(002)/I(021) ratio does seem to be affected by the four low data points in the MK-IV area (Samples 18–36). An inquiry to double check the data analysis indicates that these are legitimate results. If the PHRs also showed this effect, one might suspect that a texture was present orthogonal to a deformation-induced texture with high (110) and low (002) values. Another reason to suspect these is that they alternate between being equivalent to the rest of the database and being low; the ones that are low were all run in 2017, the others in 2018. Explanations for the difference have not been found, although the common default is to say the sample preparation may have somehow changed slightly. This may require further investigation.

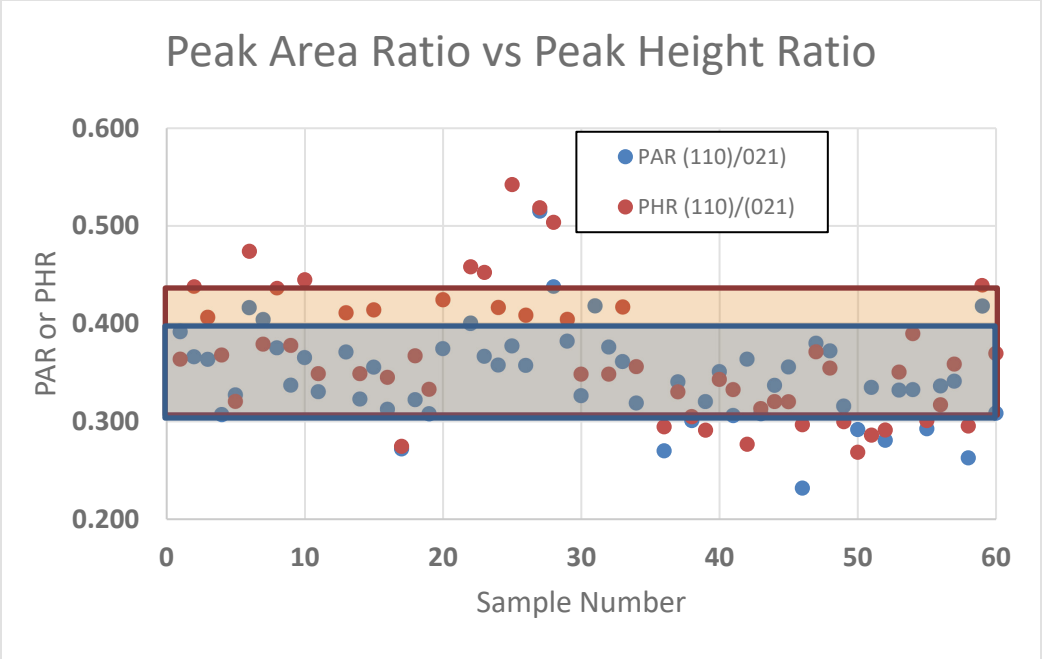

Average	0.345	0.370
STDEV.S	0.048	0.067
	PAR	PHR

Figure 10. XRD results for EBR-II legacy fuels comparing peak area ratio and peak height ration for the I(110)/I(021) ratios.

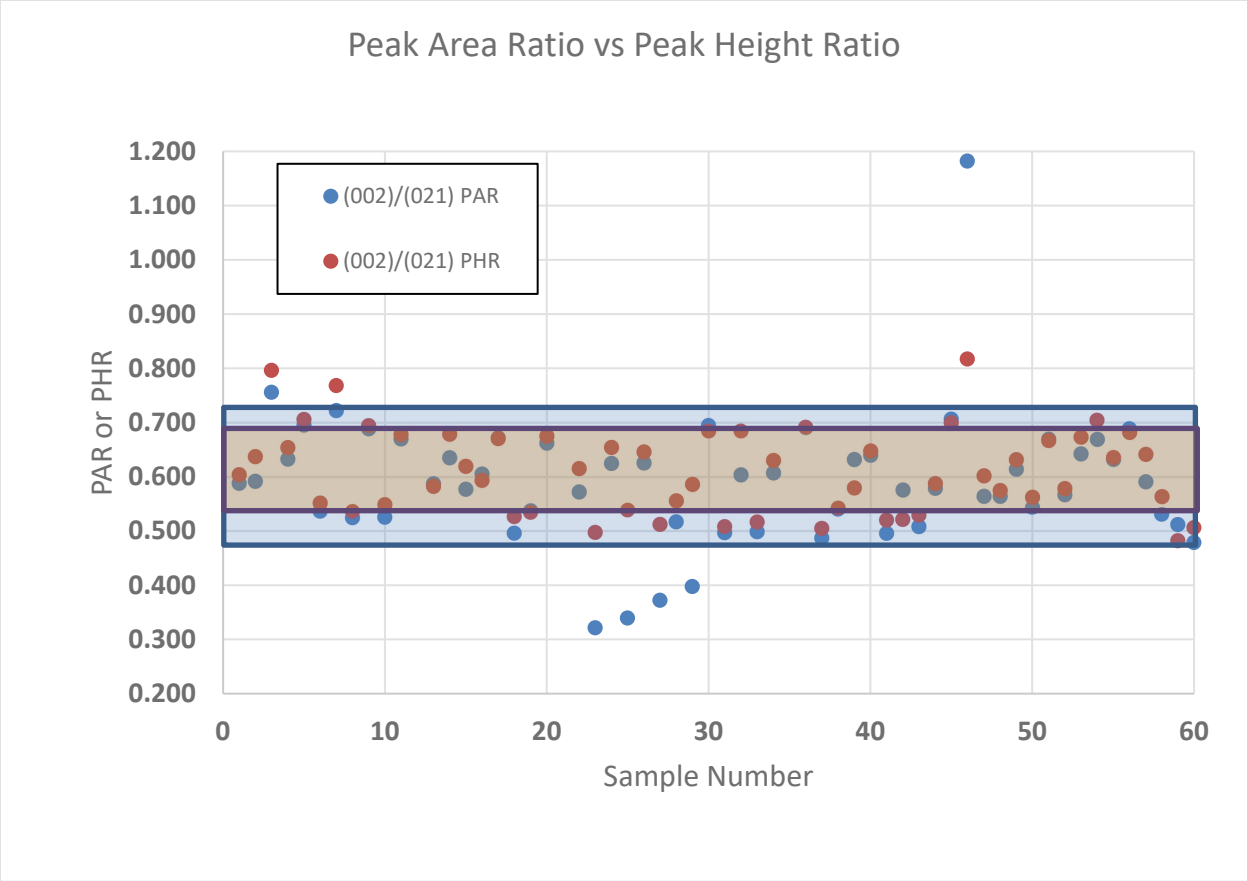

Average	0.591	0.611
STDEV.S	0.122	0.078
	PAR	PHR

Figure 11. XRD results for EBR-II legacy fuels comparing peak area ratio and peak height ratio for the I(002)/I(021) ratios.

The above were observations concerning the data. Files of the RAW data, REDUCED data, (background subtracted), and REFINED data (analyzed using other techniques, such as UZr_2 subtraction) have been transmitted to TerraPower under separate cover.

The analysis presented here is intended to provide some insight that INL has gained in reviewing the data. The intent was to provide information that may help in picking the proper XRD characteristic to represent the injection cast slugs—an XRD characteristic that may be associated with the fuel performance characteristics of this fuel.

3. XRD Characterization of Fuel Used for AFC-4B and AFC-4D Testing in the Advanced Test Reactor

3.1 Introduction

There are a few experiments being irradiated in the Advanced test Reactor (ATR) to investigate the performance of some advanced design elements of TerraPower. Part of the fuel characterization process prior to irradiation was to identify texture using XRD. This fuel resembles pure uranium with just enough alloying to effect solid solution hardening; the expectations are that its crystal structure, and XRD peak intensities, should follow that of pure uranium. The team expected that any anisotropy could be revealed by using techniques developed previously for looking at these materials [16] and later at U-5Fs.

Perhaps it shouldn't be expected to find anisotropy in as-cast samples of this material, but Riggs and Neumann did find a texture in their as-cast, low-alloy materials [17]. In the present study, however, a secondary heat treatment (particularly a beta quench treatment) was given to these materials, both for AFC-4B fuel and later for AFC-4D fuel. The full treatment was 760°C for 30 min→ water quench → 600°C for 1 hr. → water quench. The final half of the treatment is called the alpha anneal.

3.2 History of XRD Measurements

The first XRD measurements of these materials were done just before the AFC-4B experiment began irradiation. Then the AFC-4D samples were fabricated and examined a few years later. In both cases, the samples were mechanically polished prior to examination and were examined as mounted in an epoxy mount. Table 5 shows these results. The latter is not done today because of errors that can be created by the interference from the epoxy as it diffracts the x-rays [6]. The original analysis of the AFC-4B samples provided somewhat high I(110)/I(021) ratios compared to the expected ~0.73 thought to be representative of a non-textured sample of pure uranium (see Table 6). Recently, a phosphoric acid electropolish (8V for 30 sec) was used as a final polish after a re-polish from the previous exam using 1200 grit paper. Note that one of the early investigators of U-5Fs texture used 18V for 20 seconds [5].

The AFC-4B samples were unmounted, providing values (0.410–0.656) considerably less than the original ones and even less than those expected for anisotropic samples. Since the AFC fuel samples were as-cast and heat treated, uniform orientation, vs. anisotropic texture, would have been expected.

Table 6. Original AFC-4B characterization sample with XRD.

Sample	Peak Height Ratio, I (110)/I(021)
4B-1	0.820
4B-2	0.891
4B-3	0.679
4B-4	0.938
4B-5	0.817

The examination of AFC-4D fuel samples was even more interesting, as these had been fabricated and heat treated in exactly the same manner as the AFC-4B samples had been a few years earlier. However, when the samples were examined using XRD utilizing the same early methods as had been used for the AFC-4B samples, the results were as shown in Table 7. The I(110)/I(021) ratios were in general lower (0.301 to 0.625) than the AFC-4B samples had shown (0.679 to 0.938).

Table 7. AFC-4D initial/original XRD results.

Sample	I(110)/I(021)
4D-1 Sample 4	0.625
4D-1 Sample 5	0.446
4D-2 Sample 4	0.406
4D-2 Sample 5	0.301
4D-3 Sample 4	0.354
4D-3 Sample 5	0.353
4D-4 Sample 4	0.365
4D-4 Sample 5	0.434

It was first suspected that the mechanical working of the sample surface to cut and polish the samples may have been different during the second testing, since the person preparing the samples had changed. An effort was made to prepare the samples the same way earlier (AFC-4B) samples had been prepared. The results were very similar to the first try.

The research team then thought that if a sample was prepared using a surface orthogonal to the sample first tested, if the XRD results did reflect a texture through the bulk of the sample, the ratios would be much different than the original value. The sample that had produced a ratio of 0.301 was polished on an orthogonal surface, and the result was 0.428—again low, but not as low. Bulk texture was not indicated and surface preparation was again suspected. The early (1960–1970) reports had said they had used electro-polishing to ensure there was no smearing of a surface layer created by mechanical polishing. An H_2PO_4 electro-polish was used to prepare again four of the original eight samples. Moreover, all of the practices to ensure method standardization, including no use of mounting materials, were applied here.

The results are shown in Table 8, 0.378 to 0.610 for the AFC-4D samples. The AFC-4B samples, run using the newly defined methods, returned values of 0.410 to 0.656, so all of the samples for both AFC-4B and AFC-4D fell in the same range, but at a low ratio, much in the same range as did the U-10Zr legacy/archive samples. Again, there is reason to rethink, and to reestablish expected values for peak height ratios by examining uranium standards using these same methods.

Table 8. The I(110)/I(021) ratio comparing final sample polish techniques.

Sample	Electropolish	Earlier Mechanical Polish†
D1047-4B-1	0.410	0.82
ID1048-4B-2	0.609	0.891
ID1049-4B-3	0.656	0.679
ID1050-4B-4	0.525	0.938
ID1319-4D-1	0.425	0.625, 0.446
ID1320-4D-2	0.475 (0.428*)	0.406,0.301
ID1326-4D-4	0.378	0.365, 0.434
ID1329-4D-3	0.610	0.354, 0.353

*This was the sample cut from and orthogonal to 4D-2.
†Entrees with two items include both the “A” and the “B” slugs.

Comparing the (002)/(021) ratios, after electropolishing, 4B-1 had a PHR of 0.419 and 4B-2 0.513; ~0.54 is the calculated un-textured ratio.

REFERENCES

1. L. Squires, Kevin Tolman, F. DiLemma, T. Hartman, and D. Porter, "Modified Peak Ratio Method for Quantitative Texture Analysis of U10Zr Alloys," INL/EXT-4392, June 2017.
2. H. H. Chiswik, "Effects of Preferred Orientation and Grain Size on Dimensional Stability of Uranium on Thermal Cycling and Irradiation," ANL-4955 (1954).
3. E. F. Sturcken and W. R. McDonnel, "An X-ray Method for Predicting Anisotropic Growth in Uranium," *Journal of Nuclear Materials*, Vol. 7, No. 1 (1962) pp. 85–91.
4. C. M. Walter, M. H. Mueller, and J. P. Bacca, "Application of X-ray Texture Studies to Explain the Anomalous Performance of Centrifugally Bonded EBR-II Driver Fuel," *Transactions of the American Nuclear Society,* Vol. 13, No. 1, 1970 Annual Meeting, Los Angeles, CA June 28–July 2, 1970.
5. Sturcken and Wicks, "Irradiation Growth of EBR-II Fuel Pins," DP-1273 (1971).
6. K. Tolman, "U-10Zr XRD Follow-on Report: Effect of Background, Extrusion, Heat Treatment," INL/EXT-18-44349, January 2018.
7. Papesch, C., et. al, "Material Characterization Report of FFTF MFF-5 Fuel Element," INL/LTD-13-29073, Idaho National Laboratory, 2013.
8. Papesch, C., et. al, "Material Characterization Report of EBR-II Mark IV Fuel Element," INL/LTD-13-29071, Idaho National Laboratory, 2013.
9. G.B. Harris, X. "Quantitative measurement of preferred orientation in rolled uranium bars," *The London, Edinburgh, and Dublin Philosophical Magazine and Journal of Science,* 43.336 (1952) pp. 113–123, DOI: 10.1080/14786440108520972.
10. W. A. Dollase, "Correction of intensities for preferred orientation in powder diffractometry: Application of the March model," *J. Appl. Cryst.* 19 (1986), pp. 267–272.
11. "X-Ray Diffraction Texture Analysis of Uranium Alloy Fuel," PLN-5527, 2018.
12. A. H. Cash, E. W. Hughes, and C. C. Murdock, "The Structure of Crystalline Uranium," *Acta Cryst*., Vol. 14 (1963) pp. 313–314.
13. L. Squires and T. Hartmann, "Progress Report on Development of Texture Measuring Technique via XRD," INL/EXT-15-34493, March 2015.
14. L.C. Walters, G. L. Hofman, and R.H. Rohde, "Texture Studies on EBR-II, Mark-II Driver Fuel," *Trans. Am Nucl. Soc*., Vol. 17 (1973) pp. 217–218.
15. S. Kaity, J. Banerjee, S. Parida, A. Laik, and C. Basak, "Studies on fuel-cladding chemical interaction between U-10wt%Zr alloy and T91 steel," *Journal of Nuclear Materials*, Vol. 513 (2019) pp.16–32.
16. E. F. Sturcken and W. R. McDonell, "An X-Ray Method for Predicting Anisotropic Irradiation Growth in Uranium." *Journal of Nuclear Materials,* Vol. 1, (1962) pp. 85–91.
17. K. R. Riggs and N. F. Neumann, "Effect of Alloy Additions on the Quench–induced Texture of Alpha Uranium," Mallinckrodt Chemical Works, Uranium Division, MCW-1491 (April 1965).

Appendix A

Extended Data for the Legacy EBR-II Fuel Slugs

MK-III

ID	Date	Goniometer Radius [mm]	Generator [kV]	Generator [mA]	Temp. [˚C]	2θ [20˚ - 90˚]	Step Size	Step Time [sec]	Solar [rad]	Mask	Slit Size [mm]	Cu Kα1 [Å]	Spinning	a-U %	UO2 %	d-UZr2 %
1357A	Aug'18	240	45	40	25	Y	0.013	198.645	0.4	10	0.1	1.5406	Y	87.44	3.51	9.05
1357B	Apr'18	240	45	40	25	Y	0.013	198.645	0.4	10	0.1	1.5406	Y	81.29	6.4	12.32
1357B	Nov'17	240	45	40	25	Y	0.013	198.645	0.4	10	0.1	1.5406	Y	82.79	7.07	10.15
1357C	Apr'18	240	45	40	25	Y	0.013	198.645	0.4	10	0.1	1.5406	Y	81.73	8.3	9.96
1357C	Oct'17	240	45	40	25	Y	0.013	198.645	0.4	10	0.1	1.5406	Y	85.93	4.46	9.6
1357D	Apr'18	240	45	40	25	Y	0.013	198.645	0.4	10	0.1	1.5406	Y	86.73	4.3	8.97
1357E	Aug'18	240	45	40	25	Y	0.013	198.645	0.4	10	0.1	1.5406	Y	87.64	3.96	8.39
1357F	Apr'18	240	45	40	25	Y	0.013	198.645	0.4	10	0.1	1.5406	Y	84.73	5.45	9.82
1357F	Oct'17	240	45	40	25	Y	0.013	198.645	0.4	10	0.1	1.5406	Y	84.24	5.53	10.23
1357G	Mar'18	240	45	40	25	Y	0.013	198.645	0.4	10	0.1	1.5406	Y	80.45	5.62	13.93
1357G	Oct'17	240	45	40	25	Y	0.013	198.645	0.4	10	0.1	1.5406	Y	84.14	4.27	11.59
1357H	Mar'18	240	45	40	25	Y	0.013	198.645	0.4	10	0.1	1.5406	Y	83.08	5.97	10.95
1357H	Nov'17	240	45	40	25	Y	0.013	198.645	0.4	10	0.1	1.5406	Y	84.15	4.27	11.58
1357I	Apr'18	240	45	40	25	Y	0.013	198.645	0.4	10	0.1	1.5406	Y	84.26	5.87	9.87
1357I	Oct'17	240	45	40	25	Y	0.013	198.645	0.4	10	0.1	1.5406	Y	82.91	7.22	9.87
1357J	Mar'18	240	45	40	25	Y	0.013	198.645	0.4	10	0.1	1.5406	Y	85.47	5.31	9.22

Calculated patterns w/o Texture

		Random Simulated NORM	(110)	Random Simulated NORM	(021)	Random Simulated NORM	(002)	Random Simulated NORM	(111)	Random Simulated NORM	(112)	Random Simulated NORM	(131)	Height	Height	Height	Height	Height	Height
ID		Calc.(110)	Obs. Bkgnd	Calc.(021)	Obs. Bkgnd	Calc.(002)	Obs. Bkgnd	Calc.(111)	Obs. Bkgnd	Calc.(112)	Obs. Bkgnd	Calc. (131)	Obs. Bkgnd	Obs.(110)	Obs.(021)	Obs.(002)	Obs.(111)	Obs.(112)	Obs.(131)
1357A	Aug'18	11147.24	2064.127	16669.36	2064.13	8773.244	2089.93	8747.44	2167.345	7847.903	2593.218	6679.692	3011.723	6708.9	14837.25	9805.416	7818.485	7847.903	7583.769
1357B	Apr'18	12255.89	869.5482	17650.96	868.412	9877.388	867.611	8827.409	864.1865	7032.066	863.5921	5310.644	870.0039	7583.741	16207.82	10637.35	7411.725	7542.56	5789.536
1357B	Nov'17	13734.18	869.1419	19617.37	869.142	10686.27	869.142	9989.733	858.5302	7868.195	852.5623	5942.031	850.9452	8063.642	18589.58	14974.61	8418.959	9081.542	5893.172
1357C	Apr'18	12843.45	836.953	18863.71	836.953	10394.54	836.953	9252.355	834.9849	7425.708	842.883	5565.082	855.78	7314.127	18445.71	12343.97	8715.592	6834.283	5708.719
1357C	Oct'17	13031.24	925.549	18219.39	925.549	10073.81	916.089	9511.709	902.0927	7434.395	878.4984	5667.606	878.7726	6805.8	19288.46	13874.7	8566.571	8604.616	6066.675
1357D	Apr'18	12182.67	901.2853	16765.73	900.627	9345.526	903.802	9075.671	906.1291	7032.006	909.3328	5453.479	910.1927	8014.151	15907.49	9186.248	8181.482	7395.54	6311.715
1357E	Aug'18	11458.95	2051.447	17248.19	2078.25	8966.367	2078.25	9019.971	2185.457	8159.775	2635.925	6839.119	3057.839	7170.632	15586.46	12450.63	7840.682	8912.006	7621.157
1357F	Apr'18	13245.97	881.2325	18754.84	880.344	10210.36	879.648	9722.791	877.221	7612.332	878.6343	5808.385	883.3949	8562.013	18495.79	10329.04	8378.345	7645.02	6283.146
1357F	Oct'17	13313.91	908.5142	18664.91	906.638	10164.24	904.603	9807.558	895.0278	7640.986	875.9386	5832.411	875.6117	7635.989	18716.54	13270.69	8428.443	8412.886	6042.065
1357G	Mar'18	13467.86	751.6371	19553.48	750.591	11106.22	749.711	9613.061	745.9044	7621.448	745.5211	5691.371	749.3274	8217.874	17536.93	9965.507	8250.86	8052.076	6006.28
1357G	Oct'17	14454.22	883.7108	20449.94	882.163	11248.19	880.194	10369.34	870.8195	8143.078	855.6788	6166.195	859.3414	8098.663	21569.24	14893.93	8587.216	8474.324	6208.146
1357H	Mar'18	12234.53	874.0656	17455.51	873.362	9903.873	872.773	8839.611	870.3521	6996.309	872.2486	5320.45	877.4133	7722.574	17552.2	10589.19	7345.856	6552.536	5480.787
1357H	Nov'17	14454.9	885.7091	20430.03	883.583	11248.58	881.69	10378.39	871.7033	8150.443	855.7783	6172.007	859.471	8099.964	21569.24	14907.48	8587.274	8466.963	6208.217
1357I	Apr'18	12097.49	915.0705	16645.21	914.606	9305.171	914.177	8980.169	912.9387	6977.447	911.9771	5405.759	912.999	7580.915	17034.58	10898.4	8060.427	6977.447	5996.52
1357I	Oct'17	13277.81	896.6757	18683.35	894.94	10212.19	892.853	9809.525	883.2026	7644.558	863.8532	5825.602	865.9403	7265.647	19361.34	11853.66	8843.585	8525.457	6617.575
1357J	Mar'18	13129.62	885.9124	18262.66	885.071	10158.53	884.141	9528.378	880.8682	7452.381	878.8357	5704.087	880.4416	6558.365	21558.41	14735.5	8174.854	8049.345	6348.648

		Card(110) Catalog# 73		Card(021) Catalog# 100		Card(002) Catalog# 51		Card(111) Catalog# 54		Card(112) Catalog# 41					
								Peak Area Ratios (PAR)		Peak Height Ratios (PHR)		PHR w and w/o delta phase correction		Marche-Dollase Calcs	
ID		Area Int.(110)	Area Int.(021)	Area Int.(002)	Area Int.(111)	Area Int.(112)	Area Int.(131)	Area Ratio I(002)A/I(110)A	Area Ratio I(110)A/I(021)A	PHR I(110)/I(021)	PHR I(002)/I(021)	Peak-Height (110)_(021)	Mod Peak-Height (110)_(021)	MD Frac.Dir. (110)_(021)	MD Frac.Dir. (002)_(110)
1357A	Aug'18	176.2615	449.9312	264.6331	266.057	452.9926	623.518	1.501	0.392	0.364	0.604	0.3636		0.73	0.687
1357B	Apr'18	117.5489	321.1054	190.0031	171.111	380.2268	517.202	1.616	0.366	0.438	0.637	0.4377	0.5050	0.721	0.510
1357B	Nov'17	121.5457	334.4647	252.6735	183.095	438.1801	500.944	2.079	0.363	0.406	0.796	0.4060	0.4553	0.729	0.563
1357C	Apr'18	118.1117	384.9579	243.4914	218.058	372.3926	519.865	2.062	0.307	0.368	0.653	0.3678	0.4250	0.764	0.454
1357C	Oct'17	117.5111	359.3699	249.6399	204.422	456.1524	546.629	2.124	0.327	0.320	0.706	0.3202	0.3471	0.778	0.858
1357D	Apr'18	127.2756	306.0084	164.0825	188.831	354.9744	534.938	1.289	0.416	0.474	0.552	0.4740	0.5207		0.494
1357E	Aug'18	108.4422	268.6259	193.9541	154.923	371.0644	479.169	1.789	0.404	0.379	0.768	0.3790		0.753	0.813
1357F	Apr'18	129.057	343.8477	180.2665	193.2	382.2566	540.308	1.397	0.375	0.436	0.536	0.4360	0.4901	0.691	0.544
1357F	Oct'17	111.7171	331.4881	228.0253	178.998	417.2143	499.004	2.041	0.337	0.378	0.694	0.3777	0.4215	0.732	0.810
1357G	Mar'18	126.2276	345.5089	181.4563	190.84	409.3207	523.539	1.438	0.365	0.445	0.549	0.4448	0.5178	0.738	0.515
1357G	Oct'17	125.8271	381.0238	255.0182	193.228	424.6675	537.847	2.027	0.330	0.349	0.677	0.3488	0.3869	0.728	0.705
1357H	Mar'18	123.548	332.9899	195.5645	172.605	334.4627	489.329	1.583	0.371	0.411	0.583	0.4106	0.4601	0.739	0.514
1357H	Nov'17	123.9798	384.239	243.9354	200.992	494.9705	642.515	1.968	0.323	0.349	0.678	0.3488	0.3864	0.761	0.668
1357I	Apr'18	117.2241	329.7318	190.3842	182.67	338.3915	516.257	1.624	0.356	0.414	0.619	0.4135	0.4585	0.738	0.581
1357I	Oct'17	109.2113	349.7924	211.6842	200.246	426.448	540.33	1.938	0.312	0.345	0.594	0.3449	0.3870	0.792	0.410
1357J	Mar'18	104.4126	384.1279	257.8241	183.067	406.9061	565.798	2.469	0.272	0.274	0.670	0.2744	0.2965	0.773	0.698

MK-IV

ID		Goniometer Radius [mm]	Generator [kV]	Generator [mA]	Temp. [˚C]	2θ [20˚ - 90˚]	Step Size	Step Time [sec]	Solar [rad]	Mask	Slit Size [mm]	Cu Kα1 [Å]	Spinning	a-U %	UO2 %	d-UZr2 %
1347-2-1	Mar'18	**240**	45	40	25	Y	0.013	198.645	0.4	10	0.1	1.5406	Y	82.45	6.76	10.79
1347-2-1	Oct'17	240	45	40	25	Y	0.013	198.645	0.4	10	0.1	1.5406	Y	82.69	4.82	12.49
1347-2-2	Apr'18	240	45	40	25	Y	0.013	198.645	0.4	10	0.1	1.5406	Y	80.23	7.88	11.89
FS-1347-2-3	Mar'18	240	45	40	25	Y	0.013	157.845	0.4	10	0.1	1.5406	Y	87.81	3.52	8.67
1347-2-3	Nov'17	240	45	40	25	Y	0.013	198.645	0.4	10	0.1	1.5406	Y	79.58	8.68	11.74
1347-2-4	May'18	240	45	40	25	Y	0.013	198.645	0.4	10	0.1	1.5406	Y	79.29	7.78	12.93
1347-2-4	Nov'17	240	45	40	25	Y	0.013	198.645	0.4	10	0.1	1.5406	Y	81.6	5.5	12.9
1347-2-5	May'18	240	45	40	25	Y	0.013	198.645	0.4	10	0.1	1.5406	Y	80.39	7.54	12.06
1347-2-5	Oct'17	240	45	40	25	Y	0.013	198.645	0.4	10	0.1	1.5406	Y	82.81	4.04	13.15
1347-2-6	May'18	240	45	40	25	Y	0.013	198.645	0.4	10	0.1	1.5406	Y	80.25	9.58	10.17
1347-2-6	Nov'17	240	45	40	25	Y	0.013	198.645	0.4	10	0.1	1.5406	Y	80.69	8.57	10.74
1347-2-7	May'18	240	45	40	25	Y	0.013	198.645	0.4	10	0.1	1.5406	Y	82.83	7.94	9.23
1347-2-7	Oct'17	240	45	40	25	Y	0.013	198.645	0.4	10	0.1	1.5406	Y	84.75	4.49	10.76
1347-2-8	May'18	240	45	40	25	Y	0.013	198.645	0.4	10	0.1	1.5406	Y	79.13	9.12	11.75
1347-2-8	Oct'17	240	45	40	25	Y	0.013	198.645	0.4	10	0.1	1.5406	Y	84.73	4.46	10.8
1347-2-9	Apr'18	240	45	40	25	Y	0.013	198.645	0.4	10	0.1	1.5406	Y	81.36	7.04	11.59
1347-2-9	Nov'17	240	45	40	25	Y	0.013	198.645	0.4	10	0.1	1.5406	Y	84.41	7.04	8.54
1347-2-2	Oct'17	240	45	40	25	Y	0.013	198.645	0.4	10	0.1	1.5406	Y	83.45	5.91	10.64

ID		Calculated patterns w/o Texture Random Simulated NORM Calc.(110)	(110) Obs. Bkgnd	NORM Calc.(021)	(021) Obs. Bkgnd	NORM Calc.(002)	(002) Obs. Bkgnd	NORM Calc.(111)	(111) Obs. Bkgnd	NORM Calc.(112)	(112) Obs. Bkgnd	NORM Calc. (131)	(131) Obs. Bkgnd	Height Obs.(110)	Height Obs.(021)	Height Obs.(002)	Height Obs.(111)	Height Obs.(112)	Height Obs.(131)	Height Sigma +/-
1347-2-1	Mar'18	12527.36	761.8592	17824.36	760.925	10009.33	760.069	8935.956	756.8874	7063.124	757.8235	5331.734	762.8844	7213.363	18333.72	10009.3	7189.508	6910.822	6267.843	62.333
1347-2-1	Oct'17	13554.31	874.6104	18998.7	869.051	10556.44	871.53	9704.986	862.4133	7603.686	847.016	5782.276	843.6075	7290.324	20152.41	11172.75	8450.379	8462.916	6631.727	73.000
1347-2-2	Apr'18	14057.26	749.8843	20060.88	749.236	11279.62	748.4	10176.19	746.0599	7978.231	750.8595	6019.138	758.5441	8644.371	19370.51	13305.79	8271.939	7677.964	6394.894	81.000
FS-1347-2-3	Mar'18	7564.217	966.088	9815.882	964.79	5784.579	965.654	5646.509	966.1984	4450.405	967.2545	3617.775	969.384	6131.803	7531.241	7758.596	5778.117	5284.295	3423.107	63.667
1347-2-3	Nov'17	13361.29	861.9505	19303.27	856.938	10544.43	859.509	9752.965	852.3084	7676.615	845.0342	5810.266	854.8495	8532.487	17600.53	11160.75	8307.559	7676.615	6078.127	107.000
1347-2-4	May'18	10795.97	948.9289	14343.49	950.224	8089.373	946.558	8248.825	943.6683	6322.113	935.153	4995.33	933.6851	7175.976	14714.88	7788.239	6955.332	6764.473	5949.008	76.667
1347-2-4	Nov'17	13943.75	868.6252	19763.6	863.627	11073.38	865.048	10010.75	856.9151	7888.236	843.1349	5970.486	849.5526	8423.14	19020.53	12737.57	8286.573	8433.16	6105.485	94.000
1347-2-5	May'18	11052.34	948.7234	14706.93	949.793	8316.28	945.958	8395.594	942.2067	6443.728	930.1896	5085.267	927.1296	7968.439	13894.96	7918.556	6774.2	7042.577	5971.427	84.667
1347-2-5	Oct'17	13872.13	883.8346	19778.43	878.936	10903.06	880.522	9974.958	871.7567	7859.419	856.0606	5940.794	860.1586	8388.184	19261.52	12749.32	8325.489	7993.629	6489.272	80.333
1347-2-6	May'18	11329.36	921.894	15379.7	919.346	8524.456	922.308	8607.397	919.8313	6600.374	927.6831	5205.962	919.655	8162.646	14885.33	8069.627	7017.32	7298.551	6089.736	
1347-2-6	Nov'17	12447.71	876.2689	17891.21	871.755	9707.792	874.372	9092.833	866.6267	7207.876	857.0845	5455.808	864.36	8452.101	15912.88	9238.894	7627.892	7788.452	5857.666	
1347-2-7	May'18	12221.48	941.6399	16339.22	943.9	9116.639	940.023	9277.732	937.0278	7085.699	931.8251	5561.759	932.0222	7732.372	17756.83	10795.17	7618.03	7740.122	6569.464	
1347-2-7	Oct'17	13743.11	894.7168	19490.51	889.602	10792.81	890.655	10016.29	882.5318	7846.161	864.5408	5986.873	867.4631	7461.676	19748.41	13792.12	8970.203	8841.587	6292.925	
1347-2-8	May'18	11839.06	936.1656	15786.42	937.711	8845.526	933.753	8997.602	931.2841	6873.55	924.3969	5402.585	924.2107	8511.194	15887.26	8525.319	7256.475	7224.125	6214.402	
1347-2-8	Oct'17	13747.36	895.8539	19458.29	890.85	10793.1	891.922	10022.04	883.8857	7832.703	865.952	5986.944	868.717	7464.399	19748.41	13792.12	8975.447	8841.587	6292.925	
1347-2-9	Apr'18	12813.25	863.4771	18168.57	844.737	10593.14	861.885	9335.377	859.795	7321.507	866.1455	5607.661	875.7186	7952.543	17866.63	9649.698	7793.523	7321.507	6071.799	
1347-2-9	Nov'17	13890.8	903.7248	19598.64	903.237	10853.48	900.856	10293.01	893.2737	8026.577	882.499	6146.506	886.1236	7900.033	20562.32	13280.95	9595.975	8699.262	6641.822	
1347-2-2	Oct'17	14325.08	886.3089	20554.38	885.919	12098.34	866.113	10483.12	872.2681	8137.196	854.9671	6192.617	856.4309	7400.744	23015.96	16164.61	8776.618	7954.744	6646.761	

		Card(110)	Card(021)	Card(002)	Card(111)	Card(112)						
		Catalog# 73	Catalog# 100	Catalog# 51	Catalog# 54	Catalog# 41						
							Peak Area Ratios (PAR)			Peak Height Ratios (PHR)		
ID		Area Int.(110)	Area Int.(021)	Area Int.(002)	Area Int.(111)	Area Int.(112)	Area Int.(131)	Area Ratio I(002)A/I(110)A	Area Ratio I(110)A/I(021)A	Area Ratio I(002)A/I(021)A	PHR I(002)/I(110)	PHR I(110)/I(021)	PHR I(002)/I(021)
1347-2-1	Mar'18	114.2501	354.8355	175.9081	169.246	347.1062	603.995	1.540	0.322	0.496	2.724	0.367	0.526
1347-2-1	Oct'17	113.814	369.9336	198.9218	191.55	417.8234	572.628	1.748	0.308	0.538	3.005	0.333	0.534
1347-2-2	Apr'18	132.7584	354.5915	234.6441	188.324	382.5371	551.278	1.767	0.374	0.662	2.359	0.424	0.674
FS-1347-2-3	Mar'18										1.271	0.787	1.034
1347-2-3	Nov'17	129.2381	322.9438	184.8358	177.727	362.4771	487.094	1.430	0.400	0.572	2.183	0.458	0.615
1347-2-4	May'18	122.9868	335.5299	107.8205	139.177	285.4344	432.308	0.877	0.367	0.321	2.211	0.452	0.497
1347-2-4	Nov'17	128.591	359.6743	224.6307	186.803	419.2084	531.281	1.747	0.358	0.625	2.403	0.416	0.654
1347-2-5	May'18	130.6255	346.3463	117.5005	139.704	322.9552	443.595	0.900	0.377	0.339	1.845	0.542	0.539
1347-2-5	Oct'17	125.6008	351.6345	219.9792	181.704	392.6719	551.208	1.751	0.357	0.626	2.449	0.408	0.646
1347-2-6	May'18	163.7395	317.9419	118.2734	143.817	328.3769	426.964	0.722	0.515	0.372	1.928	0.518	0.512
1347-2-6	Nov'17	127.8801	292.2239	150.9223	163.293	369.706	484.556	1.180	0.438	0.516	1.985	0.504	0.556
1347-2-7	May'18	153.6907	402.258	159.799	147.446	330.1162	464.601	1.040	0.382	0.397	2.476	0.404	0.586
1347-2-7	Oct'17	113.7692	348.8936	242.3136	197.821	429.2799	526.47	2.130	0.326	0.695	2.872	0.348	0.684
1347-2-8	May'18	125.396	300.1807	149.0688	164.943	354.2362	494.475	1.189	0.418	0.497	1.974	0.507	0.508
1347-2-8	Oct'17	129.5298	344.4969	207.957	192.171	413.6564	550.735	1.605	0.376	0.604	2.871	0.348	0.684
1347-2-9	Apr'18	120.9483	334.8077	166.8135	180.616	357.3068	556.483	1.379	0.361	0.498	2.399	0.416	0.516
1347-2-9	Nov'17	113.6968	356.8175	216.6096	207.153	414.773	541.457	1.905	0.319	0.607	2.810	0.356	0.630
1347-2-2	Oct'17	116.429	431.3637	297.851	202.664	402.5479	576.485	2.558	0.270	0.690	3.400	0.294	0.691

MK-IIC (1331) and MFF 8A (1603)

ID		Goniometer Radius [mm]	Generator [kV]	Generator [mA]	Temp. [˚C]	2θ [20˚ - 90˚]	Step Size	Step Time [sec]	Solar [rad]	Mask	Slit Size [mm]	Cu Kα1 [Å]	Spinning	a-U %	UO2 %	d-UZr2 %
1331D	Apr'18	240	45	40	25	Y	0.013	198.645	0.4	10	0.1	1.5406	Y	83.95	5.55	10.5
1331E	Apr'18	240	45	40	25	Y	0.013	198.645	0.4	10	0.1	1.5406	Y	82.64	6.00	11.36
1331F	Apr'18	240	45	40	25	Y	0.013	198.645	0.4	10	0.1	1.5406	Y	81.77	5.66	12.57
1331G	Apr'18	240	45	40	25	Y	0.013	198.645	0.4	10	0.1	1.5406	Y	83.28	4.48	12.23
1331H	Apr'18	240	45	40	25	Y	0.013	198.645	0.4	10	0.1	1.5406	Y	83.26	6.31	10.44
1331I	Apr'18	240	45	40	25	Y	0.013	398.82	0.4	10	0.1	1.5406	Y	83.13	6.46	10.41
1331J	Apr'18	240	45	40	25	Y	0.013	198.645	0.4	10	0.1	1.5406	Y	83.33	6.77	9.90
1331K	Apr'18	240	45	40	25	Y	0.013	198.645	0.4	10	0.1	1.5406	Y	84.08	5.55	10.37
1331L	Apr'18	240	45	40	25	Y	0.013	198.645	0.4	10	0.1	1.5406	Y	83.53	4.81	11.63
1603A	Apr'18	240	45	40	25	Y	0.013	198.645	0.4	10	0.1	1.5406	Y	83.75	5.81	10.45
1603B	Apr'18	240	45	40	25	Y	0.013	198.645	0.4	10	0.1	1.5406	Y	84.91	5.00	10.09
1603C	Apr'18	240	45	40	25	Y	0.013	198.645	0.4	10	0.1	1.5406	Y	85.51	6.23	8.26
1603D	Apr'18	240	45	40	25	Y	0.013	198.645	0.4	10	0.1	1.5406	Y	84.5	5.77	9.73
1603E	Apr'18	240	45	40	25	Y	0.013	198.645	0.4	10	0.1	1.5406	Y	83.92	5.61	10.47
1603F	Apr'18	240	45	40	25	Y	0.013	198.645	0.4	10	0.1	1.5406	Y	82.74	6.73	10.53
1603G	Apr'18	240	45	40	25	Y	0.013	198.645	0.4	10	0.1	1.5406	Y	82.43	6.96	10.62
1603H	Apr'18	240	45	40	25	Y	0.013	198.645	0.4	10	0.1	1.5406	Y	83.72	6.19	10.09
1603I	Mar'18	240	45	40	25	Y	0.013	198.645	0.4	10	0.1	1.5406	Y	83.54	5.39	11.07
1603J	Mar'18	240	45	40	25	Y	0.013	198.645	0.4	10	0.1	1.5406	Y	83.09	6.28	10.63

ID		Calculated patterns w/o Texture Random Simulated NORM Calc.(110)	(110) Obs. Bkgnd	Random Simulated NORM Calc.(021)	(021) Obs. Bkgnd	Random Simulated NORM Calc.(002)	(002) Obs. Bkgnd	Random Simulated NORM Calc.(111)	(111) Obs. Bkgnd	Random Simulated NORM Calc.(112)	(112) Obs. Bkgnd	Random Simulated NORM Calc. (131)	(131) Obs. Bkgnd	Height Obs.(110)	Height Obs.(021)	Height Obs.(002)	Height Obs.(111)	Height Obs.(112)	Height Obs.(131)
1331D	Apr'18	6404.491	918.969	8948.192	919.134	5271.428	919.469	4837.59	924.2029	3937.296	955.9965	3177.515	972.2566	3799.783	9321.636	6359.417	3979.461	4664.704	3610.919
1331E	Apr'18	6425.7	936.5123	8947.186	936.605	5082.898	936.795	4915.862	939.9953	3966.235	958.4493	3189.866	973.3904	4039.156	10273.26	5791.112	3990.157	4421.251	3844.545
1331F	Apr'18	5793.845	942.4126	7889.186	942.59	4615.94	942.827	4472	946.4174	3619.33	970.8736	2955.33	985.906	3333.047	9586.128	5447.178	3817.431	3856.298	3667.95
1331G	Apr'18	6714.528	938.9786	9545.577	939.043	5310.745	939.198	5123.18	942.0579	4153.143	963.0955	3307.069	974.3853	4019.358	10781.87	6146.779	4153.761	4559.717	4018.935
1331H	Apr'18	6760.859	928.8414	9652.99	929.065	5321.887	929.411	5156.077	933.7225	4188.828	960.6553	3333.608	974.3165	4039.352	10648.4	6640.733	4164.87	4677.184	3900.065
1331I	Apr'18	7069.633	930.8903	9872.607	931.099	5514.04	931.458	5392.522	935.356	4336.811	959.0045	3459.001	968.9812	4021.086	10591.29	7687.828	4854.289	5260.3	3860.436
1331J	Apr'18	6970.38	928.1749	9867.196	927.309	5456.699	926.441	5300.836	923.9782	4273.592	938.7642	3411.261	971.5036	3782.629	10555.6	8793.583	5072.542	4848.302	3834.965
1331K	Apr'18	6997.514	935.301	10045.26	934.71	5469.516	934.127	5325.442	933.0783	4312.63	949.1769	3421.925	976.3587	4373.511	10197.41	6509.1	4727.125	4878.267	4007.69
1331L	Apr'18	7061.571	940.2166	10111.17	939.684	5512.717	939.209	5379.582	938.5724	4349.903	955.1424	3454.515	980.9869	4352.808	10566.95	6475.561	4684.543	5079.917	3825.544
1603A	Apr'18	13483.91	827.9169	18709.02	826.38	10736.53	795.114	9709.949	810.8313	7604.393	837.0457	5916.543	905.4119	6765.714	20643.19	13307.59	8186.127	8867.265	7172.009
1603B	Apr'18	14087.41	809.7505	19482.44	808.433	10912.2	812.414	9985.738	828.0094	7847.276	844.048	6006.784	890.8933	6817.224	23194.29	13404.91	8480.358	9190.752	7497.507
1603C	Apr'18	13253.49	851.2289	18765.42	885.177	10303.83	851.864	9794.977	850.4711	7644.498	870.28	5904.138	914.4262	6752.018	21521.66	14606.59	8755.274	9378.116	7167.627
1603D	Apr'18	14147.52	858.6917	20468.28	858.692	11068.77	863.466	10452.11	852.199	8224.283	895.4679	6266.861	892.9816	7331.759	23095.58	13730.06	8650.078	9627.356	7550.684
1603E	Apr'18	13131.73	868.2312	18483.6	835.638	10165.81	867.75	9716.373	863.3413	7564.443	878.3626	5870.227	924.588	7137.602	18728.29	12901.74	8081.967	9203.887	6979.626
1603F	Apr'18	11954.98	822.2099	17022.88	821.503	9339.404	823.91	8736.985	825.6207	6908.188	861.293	5342.423	902.8548	6554.756	15527.37	11180.59	7087.094	8618.823	6613.665
1603G	Apr'18	11864.3	830.8877	16771.29	830.195	9295.795	832.799	8749.563	834.2944	6860.76	866.2272	5345.665	909.9801	6065.067	18228.59	11883.81	7585.951	8248.968	6608.807
1603H	Apr'18	12177.73	861.1705	16974.28	859.782	9435.383	861.258	9103.249	858.3156	7044.175	870.9446	5546.012	906.4636	6174.781	17634.95	12286.91	8484.175	9059.923	7222.306
1603I	Mar'18	13462.55	823.6412	19308.04	822.578	10638.55	825.319	9666.219	825.7875	7696.107	852.3223	5832.047	888.9608	7269.482	18802.45	12352.91	8185.258	9679.593	6913.348
1603J	Mar'18	13282.95	816.9969	19120.96	782.128	10597.15	800.987	9578.012	822.4248	7599.148	842.4113	5790.1	891.8289	6758.072	20906.76	12149.01	7527.558	8745.501	7449.011

		Card(110) Catalog# 73		Card(021) Catalog# 100		Card(002) Catalog# 51		Card(111) Catalog# 54		Card(112) Catalog# 41			
								Peak Area Ratios (PAR)			Peak Height Ratios (PHR)		
		Area	Area	Area	Area	Area	Area	Area Ratio	Area Ratio	Area Ratio	PHR	PHR	PHR
ID	Date	Int.(110)	Int.(021)	Int.(002)	Int.(111)	Int.(112)	Int.(131)	I(002)A/I(110)A	I(110)A/I(021)A	I(002)A/I(021)A	I(002)/I(110)	I(110)/I(021)	I(002)/I(021)
1331D	Apr'18	56.41356	160.8155	102.8573	76.5447	211.2811	298.527	1.823	0.351	0.640	2.917	0.343	0.647
1331E	Apr'18	55.67325	182.0423	90.18937	79.3978	206.1801	285.976	1.620	0.306	0.495	3.009	0.332	0.520
1331F	Apr'18	56.62624	155.7171	89.68322	74.3044	161.1355	337.388	1.584	0.364	0.576	3.615	0.277	0.521
1331G	Apr'18	57.33358	186.2344	94.57596	82.623	211.6664	328.474	1.650	0.308	0.508	3.195	0.313	0.529
1331H	Apr'18	61.06011	181.3346	105.0316	76.4789	209.5536	332.274	1.720	0.337	0.579	3.125	0.320	0.588
1331I	Apr'18	64.97632	182.7239	129.0773	97.2734	239.9754	316.798	1.987	0.356	0.706	3.126	0.320	0.699
1331J	Apr'18	42.36376	182.8591	216.1489	107.554	197.3049	251.735	5.102	0.232	1.182	3.373	0.296	0.817
1331K	Apr'18	70.64202	185.8792	104.8977	94.9375	228.2365	333.227	1.485	0.380	0.564	2.694	0.371	0.602
1331L	Apr'18	70.74631	190.0922	107.2753	98.6883	229.4166	336.302	1.516	0.372	0.564	2.821	0.354	0.575
1603A	Apr'18	125.9419	399.1756	245.0972	203.35	483.2542	698.731	1.946	0.316	0.614	3.343	0.300	0.631
1603B	Apr'18	123.8393	424.7342	230.8875	202.178	492.8972	715.89	1.864	0.292	0.544	3.726	0.268	0.563
1603C	Apr'18	129.5039	386.9924	258.7836	206.341	476.9138	683.5	1.998	0.335	0.669	3.503	0.286	0.667
1603D	Apr'18	116.9211	416.6011	236.293	206.042	501.2569	692.814	2.021	0.281	0.567	3.435	0.291	0.579
1603E	Apr'18	117.0297	352.7093	226.4693	194.754	496.2749	654.384	1.935	0.332	0.642	2.849	0.350	0.673
1603F	Apr'18	112.4512	338.3576	226.2424	195.515	489.0172	647.52	2.012	0.332	0.669	2.565	0.390	0.704
1603G	Apr'18	105.2279	359.912	227.4563	196.18	437.9375	610.811	2.162	0.292	0.632	3.323	0.301	0.635
1603H	Apr'18	110.9676	330.2037	227.3423	210.29	491.0471	670.187	2.049	0.336	0.688	3.157	0.317	0.681
1603I	Mar'18	125.5206	368.1309	217.4976	206.223	517.0103	651.324	1.733	0.341	0.591	2.789	0.359	0.641
1603J	Mar'18	108.4497	412.8856	219.1378	193.516	465.5963	695.145	2.021	0.263	0.531	3.384	0.295	0.564

U-5Fs –Mk-IA slug material

	Date	Goniometer Radius [mm]	Generator [kV]	Generator [mA]	Temp. [˚C]	2θ [20˚ - 90˚]	Step Size	Step Time [sec]	Solar [rad]	Mask	Slit Size [mm]	Cu Kα1 [Å]	Spinning
ID-1641-EBRII-MK1A-XRD-**T**	Aug'18	240	45	40	25	Y	0.013	198.645	0.4	10	0.1	1.5406	Y
ID-1641-EBRII-MK1A-XRD-L	Aug '18	240	45	40	25	Y	0.013	198.645	0.4	10	0.1	1.5406	Y
ID-1642-EBRII-MK1A-XRD-**T**	Aug' 18	240	45	40	25	Y	0.013	198.645	0.4	10	0.1	1.5406	Y
ID-1642-EBRII-MK1A-XRD-L	Aug'18	240	45	40	25	Y	0.013	198.645	0.4	10	0.1	1.5406	Y

ID		(110) Obs. Bkgnd	NORM Calc.(021)	(021) Obs. Bkgnd	NORM Calc.(002)	(002) Obs. Bkgnd	NORM Calc.(111)	(111) Obs. Bkgnd	NORM Calc.(112)	(112) Obs. Bkgnd	NORM Calc. (131)	(131) Obs. Bkgnd	Height Obs.(110)	Height Obs.(021)	Height Obs.(002)	Height Obs.(111)	Height Obs.(112)	Height Obs.(131)
ID-1641-EBRII-MK1A-XRD-**T**	Aug'18	1527.752		1527.752		1541.232		1595.156		1921.351		2267.737	5356.331	7364.987	5032.789	4817.094	5109.88	4745.731
ID-1641-EBRII-MK1A-XRD-L	Aug'18	2255.048		2275.124		2295.199		2395.578		2819.223		3188.587	7675.498	11570.19	7956.558	7233.831	7328.012	6996.858
ID-1642-EBRII-MK1A-XRD-**T**	Aug'18	2041.642		2065.9		2078.029		2138.674		2261.764		2410.797	4819.188	6990.283	5001.123	4637.253	4505.104	4191.35
ID-1642-EBRII-MK1A-XRD-L	Aug'18	2656.754		2674.195		2691.636		2778.841		2979.184		3208.027	7034.474	10051.79	6999.592	6615.887	6941.789	6484.102

								Peak Area Ratios (PAR)			Peak Height Ratios (PHR)		
		Area	Area	Area	Area	Area	Area	Area Ratio	Area Ratio	Area Ratio	PHR	PHR	PHR
ID	Date	Int.(110)	Int.(021)	Int.(002)	Int.(111)	Int.(112)	Int.(131)	I(002)A/I(110)A	I(110)A/I(021)A	I(002)A/I(021)A	I(002)/I(110)	I(110)/I(021)	I(002)/I(021)
ID-1641-EBRII-MK1A-XRD-**T**	Aug'18	72.11618	99.43027	54.96968	90.33531	152.6485	236.9573	0.762	0.725	0.553	0.912	0.656	0.598
ID-1641-EBRII-MK1A-XRD-L	Aug'18	104.2971	156.7813	86.32152	129.0733	216.3372	361.3477	0.828	0.665	0.551	1.044	0.583	0.609
ID-1642-EBRII-MK1A-XRD-**T**	Aug'18	53.09884	80.81558	49.65382	69.9574	104.5332	147.3119	0.935	0.657	0.614	1.052	0.564	0.594
ID-1642-EBRII-MK1A-XRD-L	Aug'18	87.79192	127.5501	73.03525	109.3553	196.2092	298.0976	0.832	0.688	0.573	0.984	0.593	0.584

Added Longitudinal Samples

	Date	Goniometer Radius [mm]	Generator [kV]	Generator [mA]	Temp. [°C]	2θ [20° - 90°]	Step Size	Step Time [sec]	Solar [rad]	Mask	Slit Size [mm]	Cu Kα1 [Å]	Spinning
ID-1331-F-XRD-L	Aug'18	240	45	40	25	Y	0.013	198.645	0.4	10	0.1	1.5406	Y
HEU-10Zr Pin 1347-2-1-XRD-L	Aug '18	240	45	40	25	Y	0.013	198.645	0.4	10	0.1	1.5406	Y
HEU-10Zr Pin 1347-2-2-XRD-L	Aug' 18	240	45	40	25	Y	0.013	198.645	0.4	10	0.1	1.5406	Y
HEU-10Zr Pin 1347-2-9-XRD-L	Aug'18	240	45	40	25	Y	0.013	198.645	0.4	10	0.1	1.5406	Y

ID		(110) Obs. Bkgnd	NORM Calc.(021)	(021) Obs. Bkgnd	NORM Calc.(002)	(002) Obs. Bkgnd	NORM Calc.(111)	(111) Obs. Bkgnd	NORM Calc.(112)	(112) Obs. Bkgnd	NORM Calc. (131)	(131) Obs. Bkgnd	Height Obs.(110)	Height Obs.(021)	Height Obs.(002)	Height Obs.(111)	Height Obs.(112)	Height Obs.(131)
ID-1331-F-XRD-L	Aug'18	2359.492		2359.492		2359.492		2451.666		2666.738		2866.447	6430.493	11023.81	7705.561	7213.969	6491.942	6998.897
HEU-10Zr Pin 1347-2-1-XRD-L	Aug'18	2277.288		2338.617		2338.617		2461.275		2829.25		3135.895	8563.523	19786.75	9606.118	7888.902	8410.2	8164.884
HEU-10Zr Pin 1347-2-2-XRD-L	Aug'18	2282.803		2309.321		2335.838		2468.426		2892.705		3184.397	7904.507	17371.24	9150.828	8249.234	8169.682	7877.99
HEU-10Zr Pin 1347-2-9-XRD-L	Aug'18	2719.396		2755.299		2755.299		2898.908		3401.54		3832.368	10869.22	23219.61	12161.7	10330.68	10294.78	10258.88

								Peak Area Ratios (PAR)			Peak Height Ratios (PHR)		
		Area	Area	Area	Area	Area	Area	Area Ratio	Area Ratio	Area Ratio	PHR	PHR	PHR
ID	Date	Int.(110)	Int.(021)	Int.(002)	Int.(111)	Int.(112)	Int.(131)	I(002)A/I(110)A	I(110)A/I(021)A	I(002)A/I(021)A	I(002)/I(110)	I(110)/I(021)	I(002)/I(021)
ID-1331-F-XRD-L	Aug'18	NA	NA	NA	NA	NA	NA	NA	NA	NA	2.128	0.470	0.617
HEU-10Zr Pin 1347-2-1-XRD-L	Aug'18	NA	NA	NA	NA	NA	NA	NA	NA	NA	2.776	0.360	0.417
HEU-10Zr Pin 1347-2-2-XRD-L	Aug'18	NA	NA	NA	NA	NA	NA	NA	NA	NA	2.675	0.373	0.452
HEU-10Zr Pin 1347-2-9-XRD-L	Aug'18	NA	NA	NA	NA	NA	NA	NA	NA	NA	2.511	0.398	0.460

Appendix B

Extended Data for the AFC-4B and AFC-4D Fuel Characterization

AFC-4B and AFC-4D Characterization Samples

ID		Goniometer Radius [mm]	Generator [kV]	Generator [mA]	Temp. [˚C]	2θ [20˚ - 90˚]	Step Size	Step Time [sec]	Solar [rad]	Mask	Slit Size [mm]	Cu Kα1 [Å]	Spinning	a-U %	UO2 %	d-UZr2 %
ID1047-4B-1	May'18	240	45	40	25	Y	0.013	198.645	0.4	10	0.1	1.5406	Y	93.65	6.35	10.5
ID1048-4B-2	May'18	240	45	40	25	Y	0.013	198.645	0.4	10	0.1	1.5406	Y	91.56	8.44	11.36
ID1049-4B-3	May'18	240	45	40	25	Y	0.013	198.645	0.4	10	0.1	1.5406	Y	91.39	8.61	12.57
ID1050-4B-4	May'18	240	45	40	25	Y	0.013	198.645	0.4	10	0.1	1.5406	Y	93.08	6.92	12.23
ID1319-4D-1	May'18	240	45	40	25	Y	0.013	198.645	0.4	10	0.1	1.5406	Y	96.17	3.83	
ID1320-4D-2	May'18	240	45	40	25	Y	0.013	198.645	0.4	10	0.1	1.5406	Y	95.02	4.98	
ID1326-4D-4	May'18	240	45	40	25	Y	0.013	198.645	0.4	10	0.1	1.5406	Y	92.66	7.34	
ID1329-4D-3	May'18	240	45	40	25	Y	0.013	198.645	0.4	10	0.1	1.5406	Y	91.39	8.61	

ID		NORM Calc.(110)	(110) Obs. Bkgnd	NORM Calc.(021)	(021) Obs. Bkgnd	NORM Calc.(002)	(002) Obs. Bkgnd	NORM Calc.(111)	(111) Obs. Bkgnd	NORM Calc.(112)	(112) Obs. Bkgnd	NORM Calc. (131)	(131) Obs. Bkgnd	Height Obs.(110)	Height Obs.(021)	Height Obs.(002)	Height Obs.(111)	Height Obs.(112)	Height Obs.(131)
ID1047-4B-1	Apr'18	6404.491	918.969	8948.192	919.134	5271.428	919.469	4837.59	924.2029	3937.296	955.9965	3177.515	972.2566	3799.783	9321.636	6359.417	3979.461	4664.704	3610.919
ID1048-4B-2	Apr'18	6425.7	936.5123	8947.186	936.605	5082.898	936.795	4915.862	939.9953	3966.235	958.4493	3189.866	973.3904	4039.156	10273.26	5791.112	3990.157	4421.251	3844.545
ID1049-4B-3	Apr'18	5793.845	942.4126	7889.186	942.59	4615.94	942.827	4472	946.4174	3619.33	970.8736	2955.33	985.906	3333.047	9586.128	5447.178	3817.431	3856.298	3667.95
ID1050-4B-4	Apr'18	6714.528	938.9786	9545.577	939.043	5310.745	939.198	5123.18	942.0579	4153.143	963.0955	3307.069	974.3853	4019.358	10781.87	6146.779	4153.761	4559.717	4018.935
ID1319-4D-1	Apr'18	6760.859	928.8414	9652.99	929.065	5321.887	929.411	5156.077	933.7225	4188.828	960.6553	3333.608	974.3165	4039.352	10648.4	6640.733	4164.87	4677.184	3900.065
ID1320-4D-2	Apr'18	7069.633	930.8903	9872.607	931.099	5514.04	931.458	5392.522	935.356	4336.811	959.0045	3459.001	968.9812	4021.086	10591.29	7687.828	4854.289	5260.3	3860.436
ID1326-4D-4	Apr'18	6970.38	928.1749	9867.196	927.309	5456.699	926.441	5300.836	923.9782	4273.592	938.7642	3411.261	971.5036	3782.629	10555.6	8793.583	5072.542	4848.302	3834.965
ID1329-4D-3	Apr'18	6997.514	935.301	10045.26	934.71	5469.516	934.127	5325.442	933.0783	4312.63	949.1769	3421.925	976.3587	4373.511	10197.41	6509.1	4727.125	4878.267	4007.69

		Peak Height Ratios (PHR)		
		PHR	PHR	PHR
ID	Date	I(002)/I(110)	**I(110)/I(021)**	I(002)/I(021)
ID1047-4B-1	Apr'18	2.442	**0.410**	0.419
ID1048-4B-2	Apr'18	1.643	**0.609**	0.513
ID1049-4B-3	Apr'18	1.524	**0.656**	0.391
ID1050-4B-4	Apr'18	1.907	**0.525**	0.642
ID1319-4D-1	Apr'18	2.355	**0.425**	0.592
ID1320-4D-2	Apr'18	2.107	**0.475**	0.933
ID1326-4D-4	Apr'18	2.643	**0.378**	0.705
ID1329-4D-3	Apr'18	1.639	**0.610**	0.388

Appendix C

Setup and Analysis Parameters for XRD Characterization

The XRD characterization follows PLN-5527 [11] and stresses unmounted samples. The PANalytical Empyrean X-ray Diffractometer was used, and the set-up parameters were:

- Automatic slit system and sample spinning
- Range $10° \geq 2\theta \geq 120°$
- Increment 0.02°
- Incident beam
  - Solar 0.04 radians
  - Radius 24 cm
  - Take-off angle 6°
  - Distance to sample 14 cm
  - Irradiated length 10 mm
  - Mask No.10 (6 mm × 14 mm)
  - Fixed slit 2° (4 mm × 30 mm)
- Diffracted beam
  - Solar 0.04 radians
  - Radius 24 cm
  - Observed length 10 mm

The analysis of the data was done using the following the instructions:

For the XRD analysis using Nano-Bruker TOPAS:

1) Begin by opening the program TOPAS 4.2.
2) Import the XRD raw data file(s) using “load scan files.”
3) Check that the x-ray source parameters under “emission profile” are correct (in this case, the wavelength is CuKalpha1 = 1.540596A and CuKalpha2 = 1.544493A) or change them to the correct wavelengths of the filament material. Note, there is a Ni beta filter in this PANalytical diffractometer (i.e., no Kbeta wavelength in this case).
4) Next, choose an order of polynomial for the background under “background” (typically it will be a Chebychev 4th order or 6th order).
5) In the “instrument” section, fill in the instrument parameters or import the instrument parameters from a .par file under “load instrument details.” Please keep in mind that, unless you are doing a Le Bail refinement with a Finger et al. asymmetry correction, this software program is dependent on the instrument’s goniometer parameters (distances, soller size, etc.) rather than the parameters of the wave physics of the x-rays, such as the program GSAS.
6) In the “corrections” section, sample displacement or zero error corrections can be refined (but never at the same time). Note that this diffractometer does not have a monochromator (i.e., zero for LP factor).
7) Next, in the “miscellaneous” section, it is optional to change/adjust the type of calculation steps and constraint that may be chosen depending on the experiment.
8) Next, a structure may be chosen using the “add structure” option (rather than the peak phase option, unless a single peak refinement is needed). Note that a “good” starting structural model must be used for the structure refinement. For instance, the space group must be correct and the

lattice constants must be relatively close to the experimental lattice constants. Then repeat adding structures for other structures in a multiphase material/sample.